# 國 立 交 通 大 學

## 電子物理學系
## 碩 士 論 文

偶氮苯染料在溶液與高分子聚合薄膜中
的光致順反異構化動力學研究

Ultrafast photoisomerization dynamics of
azo dye in solution and a polymer film

研究生：許純芝

指導教授：羅志偉 教授

中華民國九十八年七月

偶氮苯染料在溶液與高分子聚合薄膜中

的光致順反異構化動力學研究

# Ultrafast photoisomerization dynamics of

# azo dye in solution and a polymer film

研 究 生：許純芝 　　　　　Student：Chun-Chih Hsu

指導教授：羅志偉　教授 　　Advisor：Prof. Chih-Wei Luo

國 立 交 通 大 學
電 子 物 理 學 系
碩 士 論 文

A Thesis
Submitted to Department of Electrophysics
College of Science
National Chiao Tung University
In Partial
Fulfillment of the Requirements
For the Degree of Master
In
Electrophysics

July 2009

Hsinchu, Taiwan, Republic of China

中華民國九十八年七月

# 偶氮苯染料在溶液與高分子聚合薄膜中
# 的光致順反異構化動力學研究

研究生：許純芝　　　　　　　　　　　　指導教授：羅志偉　教授

## 國　立　交　通　大　學
## 電子物理學系碩士班

## 中　文　摘　要

　　在本論文中，我們利用飛秒時間解析吸收光譜量測分析技術，研究偶氮苯染料Disperse Red 19在溶液與高分子聚合薄膜中的超快光致順反異構化動力行為。利用非共線性光參數放大器所產生之寬頻可見光波段的短脈衝作為激發－探測光源，我們可同時觀測激發態電子弛緩過程與分子振動行為。根據量測結果，DR19在溶液與高分子聚合薄膜中皆以～100 fs的時間尺度脫離Franck-Condon能態，在溶液與高分子聚合薄膜中的激發態弛緩時間分別約為0.63 ps與0.84 ps，而高振動能的基態分子在溶液與高分子聚合薄膜中回到低振動能態的弛緩時間分別為2.55 ps與4.43 ps，藉此時間差異可推測DR19在結構緩解過程中會受到周遭分子環境的影響。

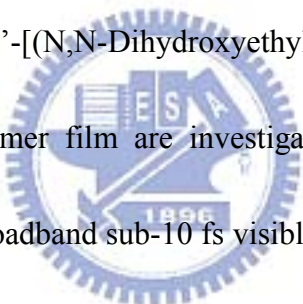# Ultrafast photoisomerization dynamics of azo dye in solution and a polymer film

Student：Chun-Chih Hsu                    Adviser：Prof. Chih-Wei Luo

## National Chiao Tung University

## Institute of Electrophysics

## Abstract

The photoisomerization of 4'-[(N,N-Dihydroxyethyl)amino]-nitroazobenzene (Disperse Red 19) in solution and in polymer film are investigated by femtosecond time-resolved absorption spectroscopy. Using broadband sub-10 fs visible pulses, the dynamics of electronic relaxation and molecular vibrations are observed in both samples. The motion of a wavepacket in the excited state out of the Franck-Condon state occurs on the time scale of ~100 fs. The excited state relaxation occurs with time constant of 0.63 ps in solution and 0.84 ps in polymer films. For a solution and a polymer film, the vibrational cooling in the ground state proceeds are 2.55 ps and 4.43 ps, respectively, suggesting that the isomerization dynamics are sensitive to the molecular environments. To the best of our knowledge, this work is the first experimental observation for the ultrafast processes of DR19 in different molecular environments.

# Acknowledgement

# Contents

# List of Figures

# List of Tables

# Chapter 1
# Introduction

## 1.1   Introduction of Azobenzene

Photochromism phenomena have become one of the most active areas of physical chemistry. It is a reversible transformation of a chemical species induced by absorption of electronmagnetic radiation between two forms. During the photoisomerization, various physical and chemical properties change, such as geometrical structure, absorption spectra, refractive index and dielectric constant. Among various photochromism reactions, trans-cis photoisomerization is one of the most fundamental and widely investigated photochemical reactions. Azobenzene and its derivatives are typical molecules showing trans-cis photoisomerization. In 1937, the photoisomerization reaction of azobenzene was first reported by Hartley [1]. From then on, a strong interest in azo compound rose, and the isomerization process was extensively investigated by various experimental methods such as UV-visible absorption [2, 3], Raman spectroscopy [4-6], and NMR [7]. Moreover, it was studied by theoretical modeling and calculations [8-10]. These studies were devoted to establish the reaction mechanism.

It is well known that the trans-azobenzene in the ground state with an absorption spectrum consisting of a weakly allowed transition to n-$\pi$*($S_1$) state and a strongly allowed transition to $\pi$-$\pi$* ($S_2$) state [11] (Shown in Figure 1-1). Excitation to either of these states results in the photoisomerization to cis-azobenzene, but excitation to $S_2$ state giving the lower
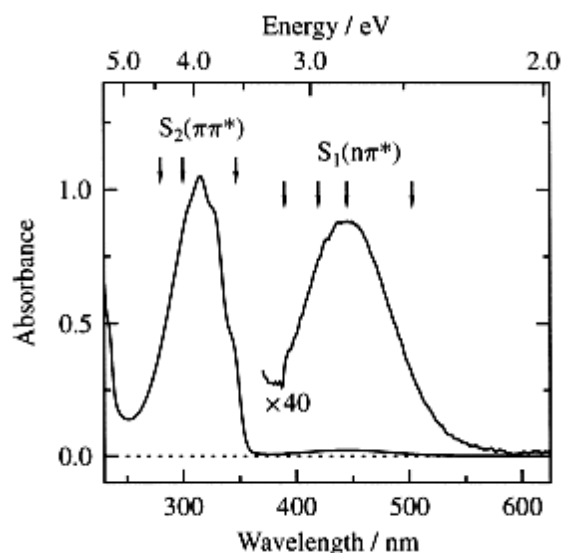
Figure 1-1 Steady-state UV-Visible absorption spectrum of trans-azobenzene in hexane [11].

quantum yield of photoisomerization [12, 13]. In contrast, the absorption spectrum of cis-azobenzene in ground state consisting of a moderate $S_2$ transition at 290 nm and a weaker $S_1$ transition at 434 nm [3, 14]. The cis isomer can be reversibly by UV light or heat, and isomerization readily occurs at room temperature [13, 15].

Since trans and cis isomers exhibit spectrally well-separated absorption band in the UV-visible absorption spectrum, reversible photochromism between the two conformations is possible. So azobenzene and its derivatives have been considered as an attractive candidate for various photonics applications such as optical switches [16, 17], high-density optical memory storage devices [18, 19], waveguide media material [20], and light-driven molecular scissors [21]. Determining the distinct absorption bands of the trans- and cis-isomers for selective conversion and understanding the isomerization mechanism and dynamics are of great interest for these applications. However, there is still an argument about the isomerization mechanism [22-24].
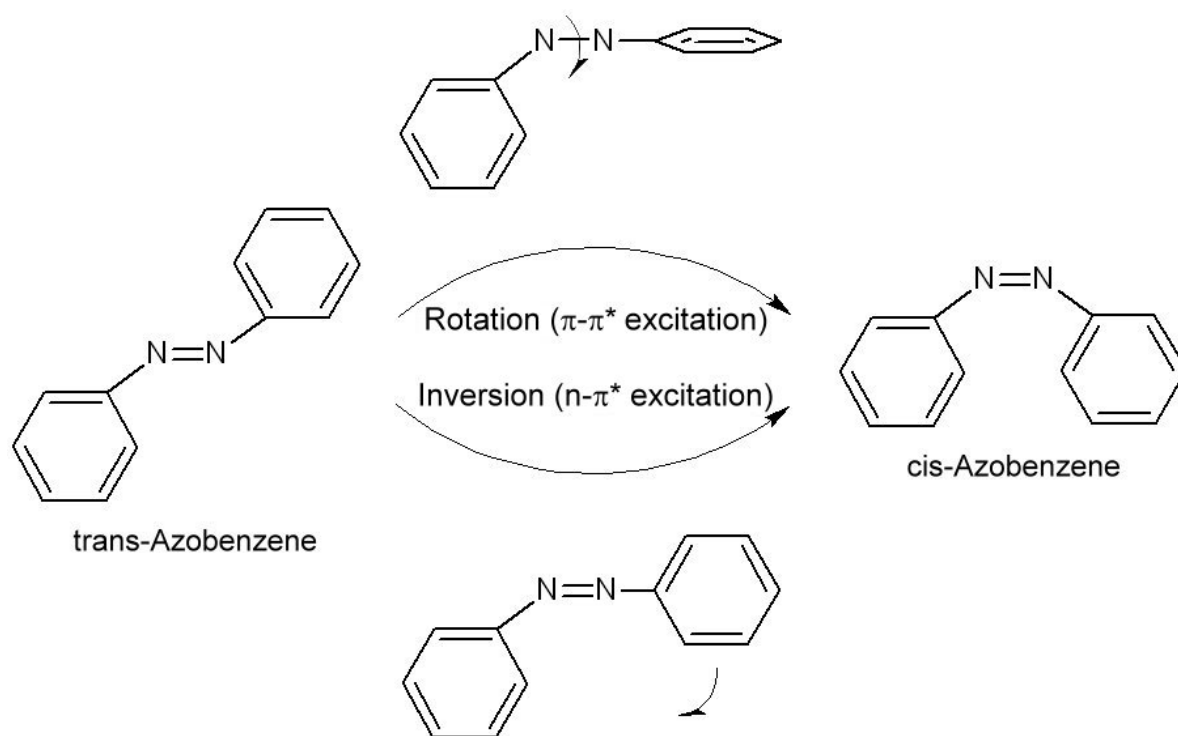
Figure 1-2 A scheme of generally accepted model of photoisomerization.

Over the last few decades, the trans-cis photoisomerization in azobenzene and related issues have been extensively studied. It has been proposed to proceed with two different mechanism, i.e. rotation and inversion which depends on the excitation wavelength [11, 13]. Figure 1-2 shows the schematic diagram of generally accepted model of photoisomerization. After UV excitation to the higher-energy π-π* (S$_2$) state, isomerization proceeds with a rotation around the N=N double bond, similar to the isomerization of widely investigated stilbene [25]. On the other hand, after visible excitation to the lower-energy n-π* (S$_1$) state, conversion between the isomers take place via the in-plane inversion of phenyl ring at one of the two N-atoms. Azobenzene has lone pair electrons on the nitrogen atoms, and thus the n-π* electronic transition is observed in addition to the π-π* transition, which may result in isomerization dynamics different from those of widely investigated stilbene [26].

Although the isomerization process was studied for a long time using various measuring methods, the details of this isomerization process must be revealed by theultrafast techniques. Due to the development of ultrashort optical spectroscopy, it enabled us to observe dynamic processes in molecules [27]. In order to investigate the isomerization dynamics of azobenzene, the trans-azobenzene in different solvents with both $\pi$-$\pi^*$ and n-$\pi^*$ excitation has been studied. For $\pi$-$\pi^*$ excitation, Lednev *et al*. observed biexponential decay with lifetimes of 0.9 and 13 ps (solvent-dependent) and interpreted the observed dynamics in the rotational mechanism [28]. The shorter-time-scale process is assigned to the relaxation of $S_2$ excited state, and the longer-time-scale process is attributed to the internal conversion of an intermediated state into ground state. For the n-$\pi^*$ excitation with different wavelength, moreover, the transient lifetimes with 0.6 ps and 2.5 ps were observed [11]. Fujino *et al*. presented the results of time-resolved fluorescence experiments that denied the rotational mechanism, and proposed that photoisomerization always occurs in the $S_1$ state [22].

Azobenzene derivatives also exhibit photoinduced reversible isomerization. The mechanism of photoisomerization of azobenzene has been widely investigated, but there are less studies on its derivatives. Compared with azobenzene, some push-pull derivatives show the faster thermal isomerization rate [15] and relatively sensitive to solvent polarity [29, 30]. Adding electron-donating group in one benzene ring raises the groud-state inversion barrier height and makes rotation be the preferred pathway of isomerization. Conversely, electron-withdrawing groups were found to lower the same barrier [31]. Figure 1-3 shows the energy diagram of substituted azobenzenes on the basis of theoretical calculations. After both $\pi$-$\pi^*$ and n-$\pi^*$ excitations, the isomerization may proceed via the rotation pathway in the majority.
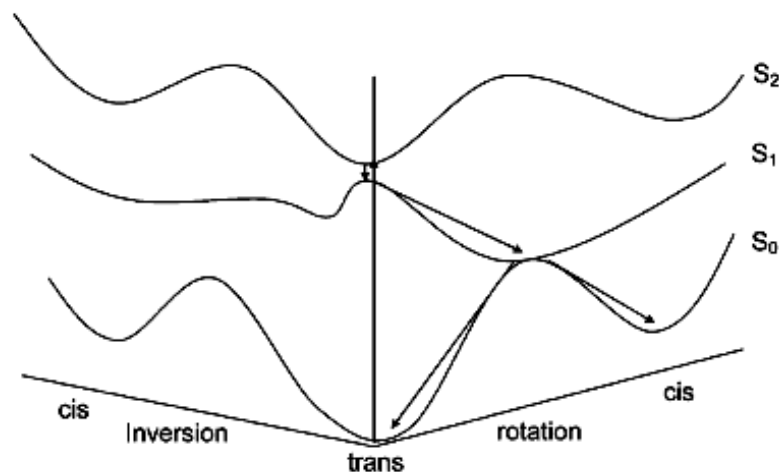
Figure 1-3 A scheme of the trans→cis isomerization process for Azon, Azonco and

AzoNO$_2$NH$_2$ [31].

## 1.2 Motivation

In order to estimate and improve azobenzene derivatives in optical storage and switching performance, it is essential to find out how molecular structure and the molecular environment affect the photoisomerization reaction. Recently, most studies have been carried out in solution, and relatively little researches in solid state. It should be emphasized, however, that most applications require performing in solid state. Therefore, understanding how molecular environment affects the isomerization process will be much useful for the synthesis of the desired materials. With tunable broadband sub-10 fs visible pulses, we can observe the relaxation dynamics and real-time frequencies of molecular vibrations in the ground state and in the excited state. In brief, the motivation of this study is to distinguish the ultrafast dynamics between solution and solid samples by investigating the real-time spectroscopy of molecular system.

# Chapter 2

# Preparation and characterization of samples

## 2.1  Preparation of samples

Disperse red 19 (DR19; Dye content 95%), bought from Sigma-Aldrich Co., was served as the azobenzene dye and used after re-crystallization. Trimethylolpropane triglycidyl ether (TMTE; technical grade) and 1, 2-Diaminopropane (DA; 99%) served as monomer and harden agent, respectively, to form epoxy resin, were obtained from Sigma-Aldrich and used as received. All the chemicals were stored in a dry box at room temperature. Figure 2-1 shows the chemical structures of all compounds.
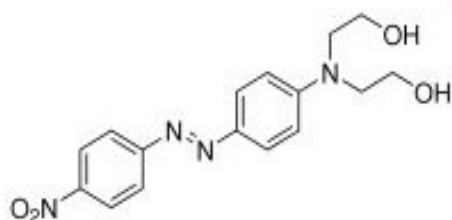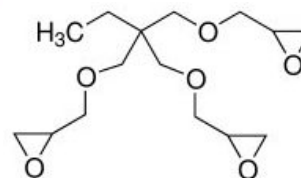


4'-[(N,N-Dihydroxyethyl)amino]          trimethylolpropane triglycidyl ether
-nitroazobenzene   (DR19)                              (TMTE)
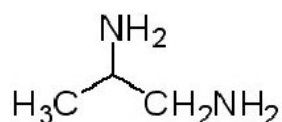


1,2-Diaminopropane
(DA)

Figure 2-1 Chemical structures of all compounds used in this study.

In order to study the characteristics of azobenzene dye in different environment, liquid state samples and solid polymer film samples were prepared in this research. For liquid state samples, DR19 molecules with concentration of 0.1 wt% were dissolved in TMTE completely through ultrasonic bath at 60℃ for 2 hours. The solution was then percolated through a syringe filter with a hole size of 0.2 μm. After these steps, the percolated solution was ready for the following measurements.

The solid polymer film samples were prepared by the doctor-blade method. First, DR19 molecules were added into DA. The solution was treated with ultrasonic bath for 10 minutes until the DR19 dissolved. Then, TMTE was added to the solution with mole ratio 1:1 between TMTE and DA, and the weight percentages of DR19 was kept at 0.1%. The solution was stirred at 60℃ for 50 minutes until it became homogeneously viscous solution. Further, the doctor-blade approach was used to cast the polymer solution on a flat glass. The samples were then polymerized in a vacuum oven at 45℃ for 24 hours to form the solid polymer film. The average thickness of the solid dry films were measured to be 0.5 mm (for pump-probe measurements) and 0.3 mm (for PL and Raman spectrum measurements), respectively. All liquid and solid samples were stored in sealed vials and dry box, respectively, in the dark state before use.

## 2.2　Optical properties of DR19 in solution and polymer films

### 2.2.1 UV-vis absorption spectra

UV-vis absorption spectra were performed on a HITACHI U-3310 spectrometer using tungsten iodide and deuterium lamp as light sources. The absorbance measurements of solution samples carried out in a quartz cell with the size of 1 cm. The absorption spectra of DR19 solutions and polymer films at room temperature are shown in Figure 2-2 (the contribution from the solvent and quartz cell was subtracted), and the spectra is dramatically different from azobenzene. Due to the charge transfer character of the transition, e.g. intramolecular and intermolecular electron transfer reaction, the dipole moment increases. Hence, the electronic charges redistribute in the excited state and results in the donor/acceptor substitution of azobenzene with shifting the π-π* band to longer wavelengths [13]. The absorption peaks in spectrum are at 494 nm and 500 nm for the solution and films, respectively, which are assigned to the strongly allowed π-π* transition. The weak n-π* absorption, forbidden in the strictly planar molecules by symmetry selection rules and insensitive to donor/acceptor substitution, is not explicitly observed in the spectra because it is buried in the strong π-π* band. In order to obtain large overlap between the laser spectrum and π-π* absorption band tail of the samples, the higher concentration samples were used for the pump-probe experiments. On the other hand, the lower concentration samples were used for the measurements of photoluminescence spectra and Raman spectra.
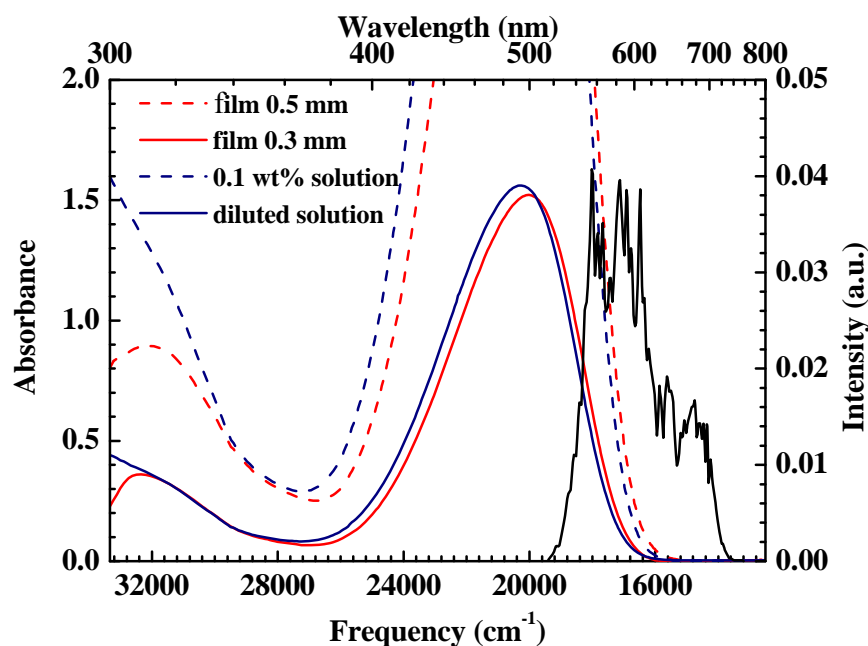
Figure 2-2 Absorption spectra of DR19 dispersed in solution and a polymer film. The spectrum of NOPA (noncollinear optical parametric amplifier) output (black curve).

## 2.2.2 Photoluminescence spectra

Photoluminescence spectra were performed on the home-built micro-PL system using He-Cd laser. The 325 nm UV line was used as the excitation light source with the power of 5 mW. The fluorescence emission spectra of DR19 in solution and polymer films at room temperature are shown in Figure 2-3, and the corresponding absorption spectrum (dash line) in each sample is also included to illustrate the Stoke's shift. The position of the maximum emission wavelength of DR19 in solution and polymer films is at 586 nm and 548 nm, respectively. It is worth to mention that the intensive fluorescence peak around 754 nm in solution case is ascribed to the fluorescence emission of the solvent (see Figure 2-4). Additionally, the spectrum in the short wavelength range is dominated by the solvent effects. The main fluorescence band of DR19 in a polymer film shows a good mirror image of the absorption band, and the major component is closely related to $\pi$-$\pi^*$ fluorescence since the n-$\pi^*$ fluorescence is extremely insensitive in push-pull derivatives.

9
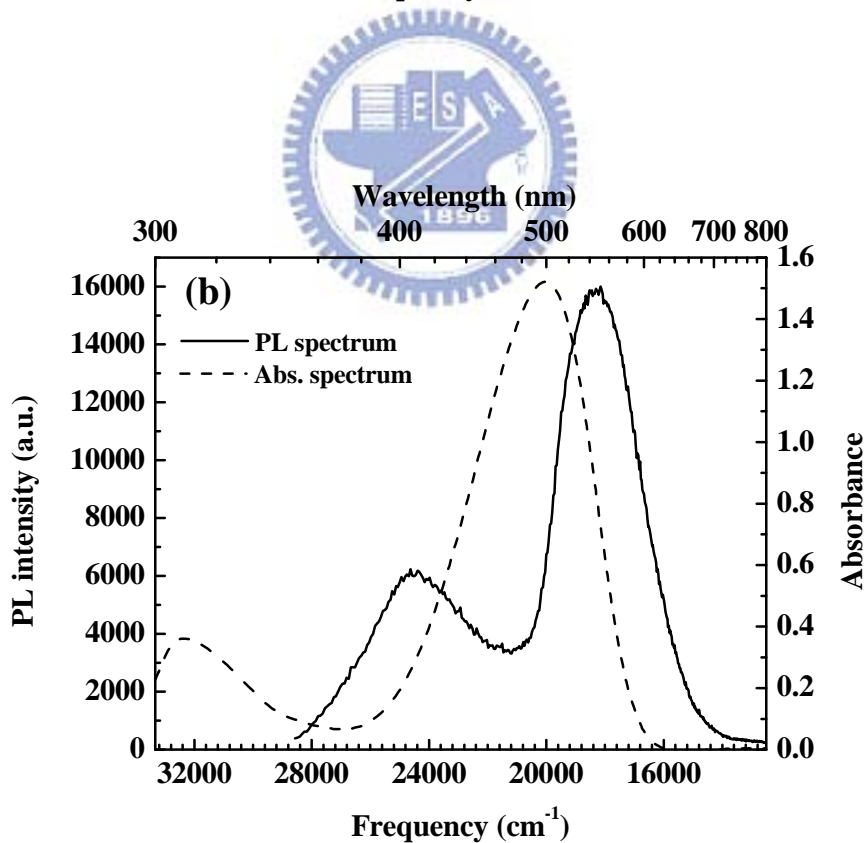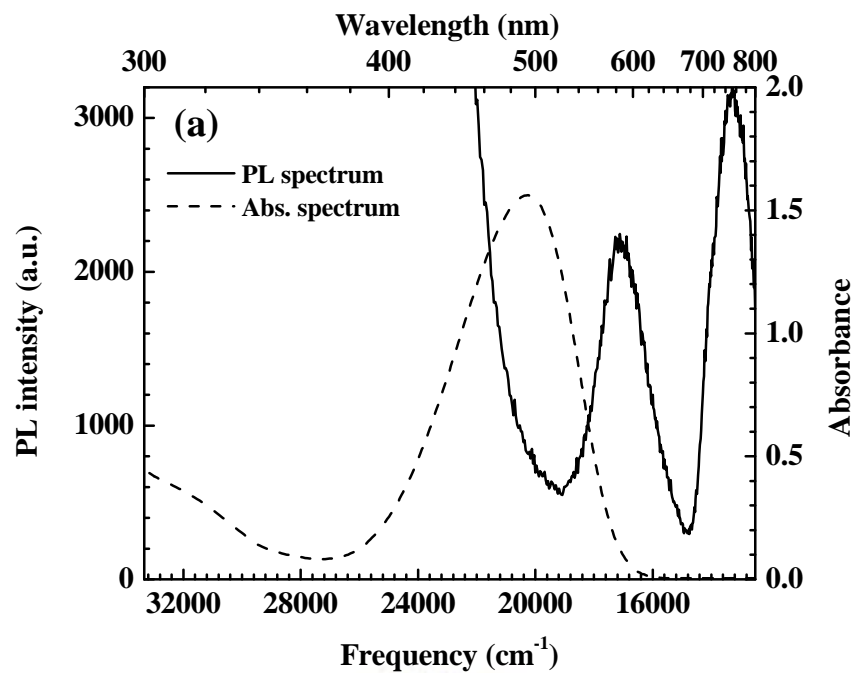
Figure 2-3 Photoluminescence spectrum of DR19 in (a) solution and (b) a polymer film.
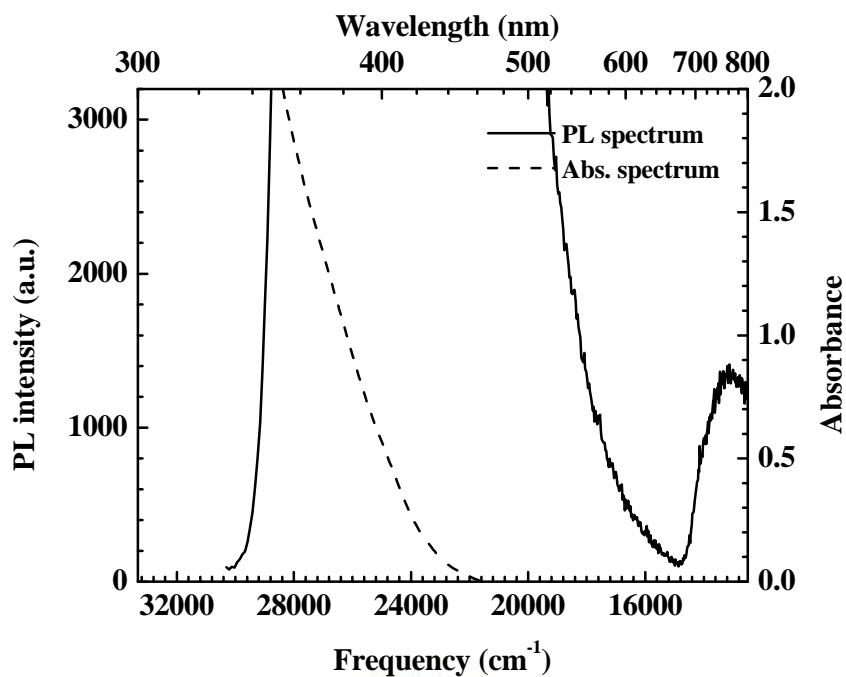
Figure 2-4 Photoluminescence spectrum of TMTE.

## 2.2.3 Raman spectra

Raman spectra were carried out with a micro-Raman spectrometer ( Horiba Jobin Yvon, Labram HR 800) with 514 nm excitation. Data was accumulated for 30 seconds in each measurement. Figure 2-5 shows the typical Raman spectra of DR19 in solution and a polymer film. Table 2-1 presents the experimental Raman frequencies of the relevant vibrational modes with the corresponding assignments. Since the molecular structure of DR19 is similar to 4-nitro-4'-dimethylaminobenzene (DA), these vibrational modes are extracted from the literature with Raman spectra of DA and other relative azo compounds [32- 34].

| Mode | $\omega_v$ /cm$^{-1}$ (in solution / polymer film) | Approximate assignments[a] |
|---|---|---|
| $\nu_1$ | 1107 / 1103 | $\nu$ (C-C) + $\delta$ (C-C) + $\nu$ (C-N)$_{NO}$ |
| $\nu_2$ | 1140 / 1139 | $\nu$ (C-N) + $\delta$ (C-C) + $\nu$ (C-C) |
| $\nu_3$ | 1200 / 1195 | $\nu$ (C-C) + $\nu$ (C-N) + $\delta$ (C-C) |
| $\nu_4$ | 1343 / 1338 | s. $\nu$ (NO$_2$) + $\nu$ (C-N)$_{NO}$ |
| $\nu_5$ | 1391 / 1390 | $\nu$ (N=N) + $\nu$ (C-N) + $\nu$ (C-C) |
| $\nu_6$ | 1426 / 1422 | $\nu$ (C-C) + $\nu$ (N-O) + $\delta$ (C-N) |
| $\nu_7$ | 1448 / 1447 | $\nu$ (C-C) + $\delta$ (C-N) |
| $\nu_8$ | 1593 / 1592 | $\nu$ (C-C) + $\delta$ (C-C) |

Table 2-1 Vibrational assignments of DR19 in solution and a polymer film.
[a] $\nu$, stretch; $\delta$, in-plane bend; s., symmetric

Resonance Raman spectroscopy has been used to study the solvent effects on molecular structure of DA [35]. The results indicate that enhanced charge transfer character in various solvents may cause more structure distortions following photoexcitation to the charge transfer state. In this work, the vibrational frequency shifts between the solution and polymer film samples is attributable to the different components of intra- and inter-molecular charge transfer reactions which depends on the surrounding environment. In both samples, mode $\nu_4$ assigned to the NO$_2$ symmetric stretching is the most intense Raman peak, followed by mode $\nu_5$ and $\nu_6$ corresponding to N=N stretching and C-C stretching. A few more peaks with weak intensity at 819, 860, 928, and 1008 cm$^{-1}$ observed in the solution case are assigned to C-C in-plane bending, C-H out-of-plane bending, C-C stretching, and C-C in-plane bending, respectively, while they are not clearly observed in the polymer film samples.
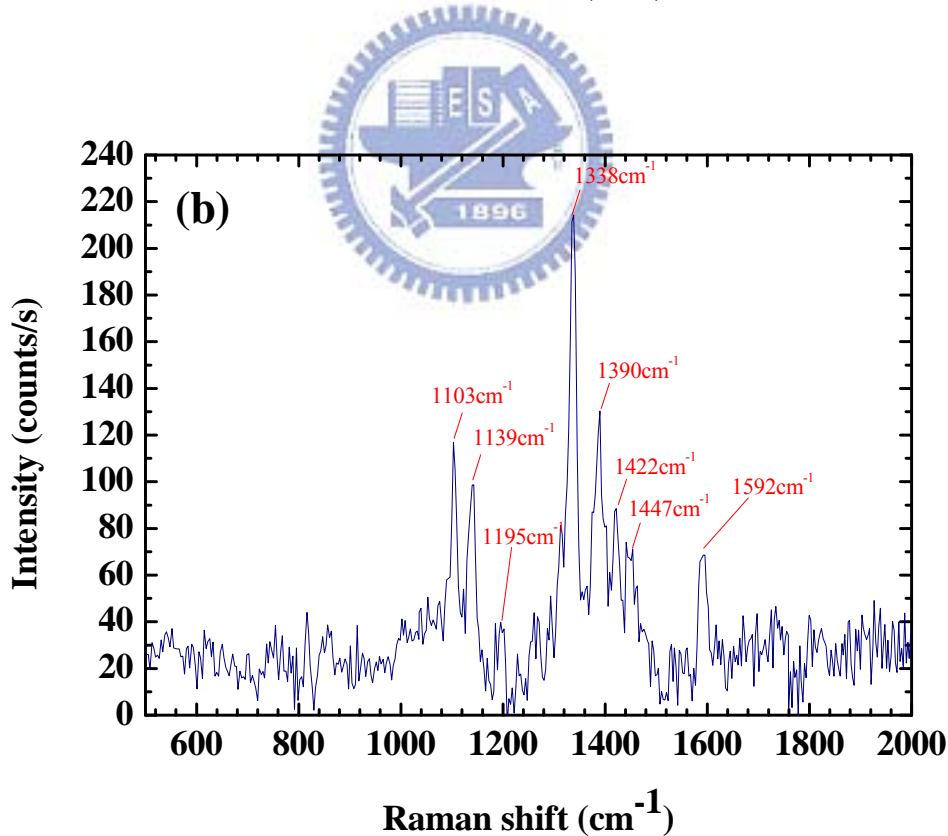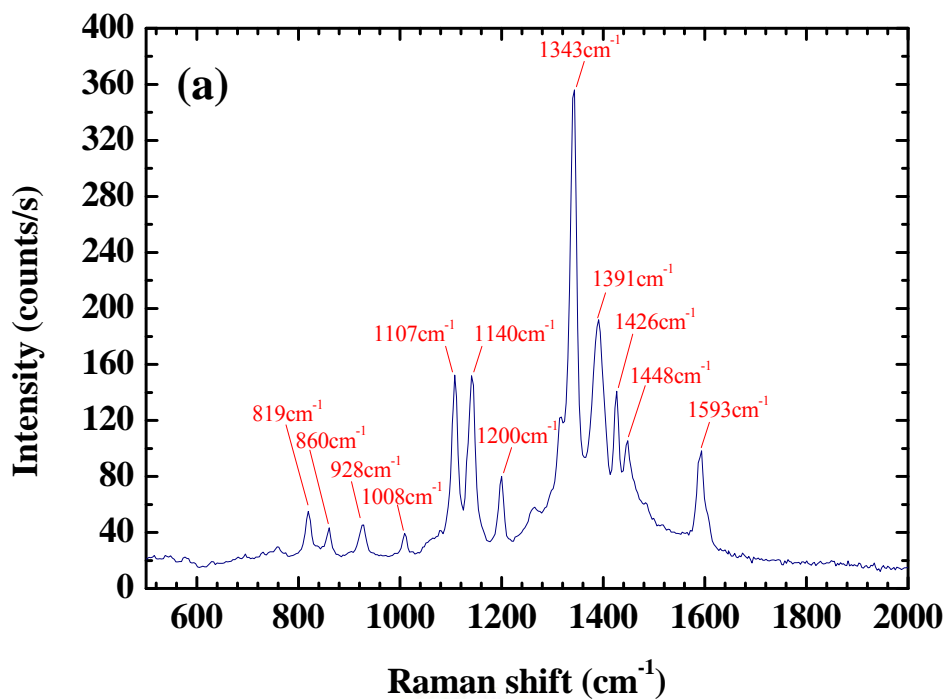
Figure 2-5 Raman spectrum of DR19 in (a) solution and (b) a polymer film with 514nm excitation.

# Chapter 3

# Experimental method and setup

## 3.1 The principle of pump-probe technique
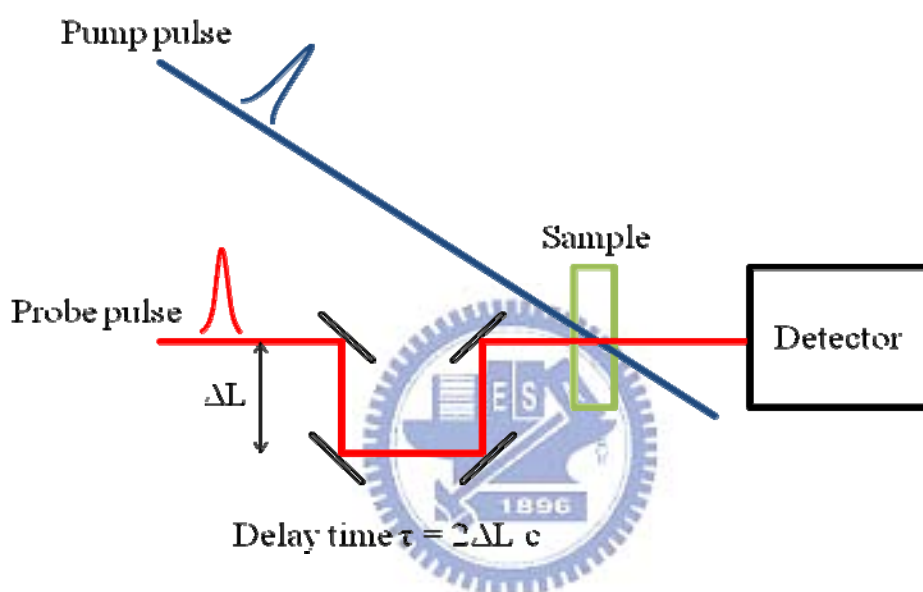


Figure 3-1 Scheme of a pump-probe experiment.

Pump-probe measurements of transient transmittance and reflectivity are the most straightforward methods for exploring ultrafast processes on a time scale of femtosecond or picosecond. The typical scheme of a pump-probe experiment is shown in Figure 3-1, both pump and probe beams are synchronized with a period longer than the lifetime of an ultrafast process. The probe pulses are typically attenuated by a factor of 10 with respect to the pump pulses, and then we can assume that it will not perturb the sample. One of the pulse replicas is sent to a fine delay line with a computer controlled stage. After pump pulses perturb the sample, the probe pulses will be affected by the pump-induced changes at delay time $\tau$. The delay time $\tau$ is adjusted by the delay line. While the probe pulse interacts with the perturbed

sample, the characteristics of the probe pulse will be modified by the perturbed sample such as the transmittance or reflectivity changes as a function of delay time τ between pump and probe pulses as shown in Figure 3-2.
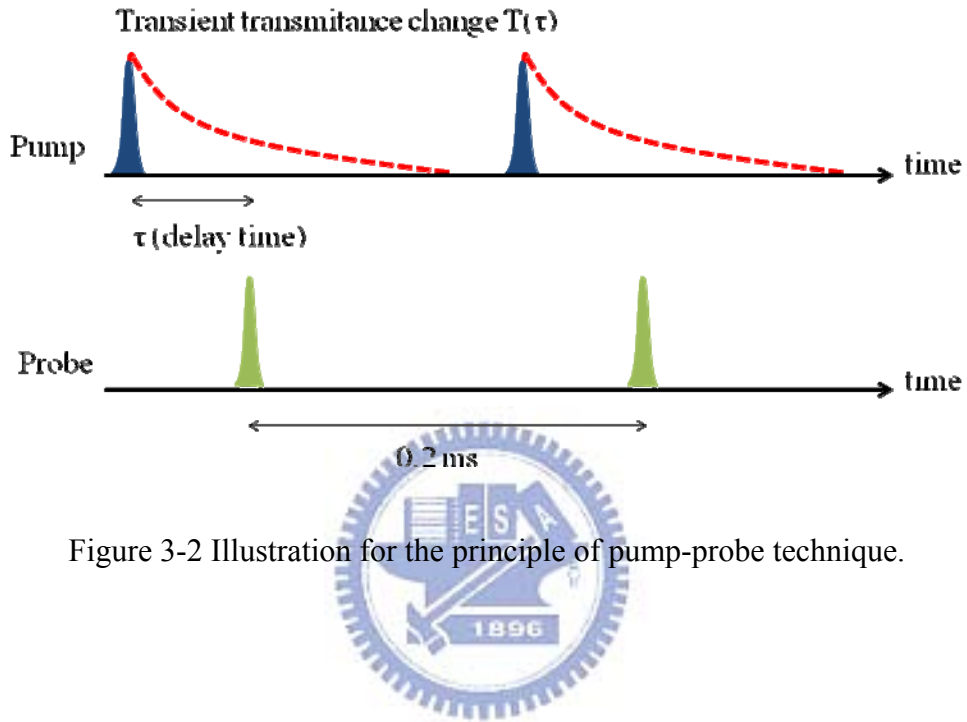


Figure 3-2 Illustration for the principle of pump-probe technique.

For recording the small changes in transmittance or reflectivity, the pump-probe experiments are commonly carried out with a lock-in amplifier (LIA). Usually the pump beam is modulated by a chopper, and the intensity of probe pulses is detected by the photodiode and then the signal of photodiode is fed to the LIA. The signal in a LIA is mixed with the frequency and phase of a chopper. Then, the output signals of LIA were changed by the ultrafast event n(τ) induced by pump pulses, i.e. a AC signal ($\Delta I(\tau)$) is added to a DC signal ($I_0$). By varying the delay time τ between pump and probe pulses, $\Delta I(\tau)$ will change as a function of delay time. Finally, the AC signal should be divided by the DC component for discriminating fluctuations of the laser. According to the relation,

$$\frac{\Delta T}{T} = \frac{T_{\text{Pump}\atop\text{open}} - T_{\text{Pump}\atop\text{closed}}}{T_{\text{Pump}\atop\text{closed}}} = \left[\left(\frac{I_t}{I_i}\right)_{\text{Pump}\atop\text{open}} - \left(\frac{I_t}{I_i}\right)_{\text{Pump}\atop\text{closed}}\right] \Bigg/ \left(\frac{I_t}{I_i}\right)_{\text{Pump}\atop\text{closed}}$$

$$= \frac{(I_t)_{\text{Pump}\atop\text{open}} - (I_t)_{\text{Pump}\atop\text{closed}}}{(I_t)_{\text{Pump}\atop\text{closed}}} = \frac{\Delta I}{I_0}$$

where $(I_i)_{\text{Pump}\atop\text{open}} = (I_i)_{\text{Pump}\atop\text{closed}}$ and $(I_t)_{\text{Pump}\atop\text{closed}} \equiv I_0$. One can obtain the relative changes in transmittance $\Delta T/T$ with the order of $10^{-6}$ by directly measuring the $\Delta I/I_0$, and $\Delta T/T$ is independent of the intensity of incident light $I_i$.

In a transmission pump-probe experiment, the data are presented in form of transient transmittance changes $\Delta T/T$, and there are three different types of signals may be detected: (1) ground state photobleaching (PB), (2) stimulated emission from the excited state (SE), and (3) photoinduced absorption from the excited state (PA) [36]. Figure 3-3 shows a scheme of energy levels in a molecular system, indicating the possible signals observed in the pump-probe experiments. The pump pulses decrease the population of electrons in the ground state, then the transmittance increase ($\Delta T/T > 0$) due to the decrease of absorption for probe pulses at photon energy = the difference between the ground state ($S_0$) and the first excited state ($S_1$), i.e. the ground state photobleaching (PB). When a probe photon with the suitable energy passes by the excited molecule system, it can stimulate the excited molecule to emit a photon and return to the ground state; what is called stimulated emission (SE) occurs at probe photon energy equal or lower than the energy of ground state absorption, also giving rise to a transmittance increase ($\Delta T/T > 0$). Moreover, the so-called photoinduced absorption (PA) results in a transmittance decrease ($\Delta T/T < 0$), which is possibly to occurre at any probe photon energy. It depends on the higher energy levels ($S_n$, $n > 1$) in the molecular system.
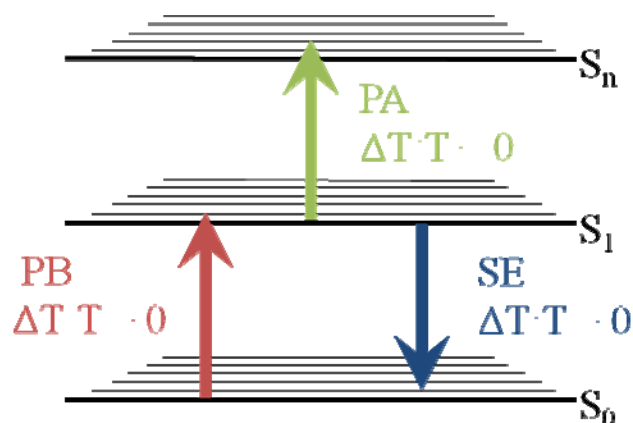
Figure 3-3 Scheme of energy levels in a molecular system with the possible absorption and emission processes.

## 3.2 Experimental setup

For the pump-probe measurements, a noncollinear optical parametric amplifier (NOPA) [37-39] was used as a light source as shown in Figure 3-4. The pump source of a NOPA system was a regenerative amplifier (Coherent, Legend L-USP-1K-HE) with the central wavelength of 800 nm, the pulse duration of 30 fs, the repetition rate of 5 kHz, and the average output power of 2.3 W. The output light of regenerative amplifier was split into two beams by a beam splitter. The fraction of output light was doubled in frequency by a BBO crystal and used as the pump for NOPA. On the other hand, the remainder light was focused into a sapphire plate to generate white-light continuum as the seed for NOPA. The output pulses from the NOPA were compressed with an optical pulse compressor composed of a diffraction grating telescopic dispersion line, specially designed multiplayer dielectric chirped mirrors, and a computer-controlled flexible mirror. After the compressor, the laser pulses were separated into two beams, one was used as a pump beam, the other was used as a probe beam after passing through an optical delay line. The setup was optimized to obtain pump and probe energies of 8 and 0.8 nJ, respectively. Both of pump and probe pulses were shorter than 10 fs
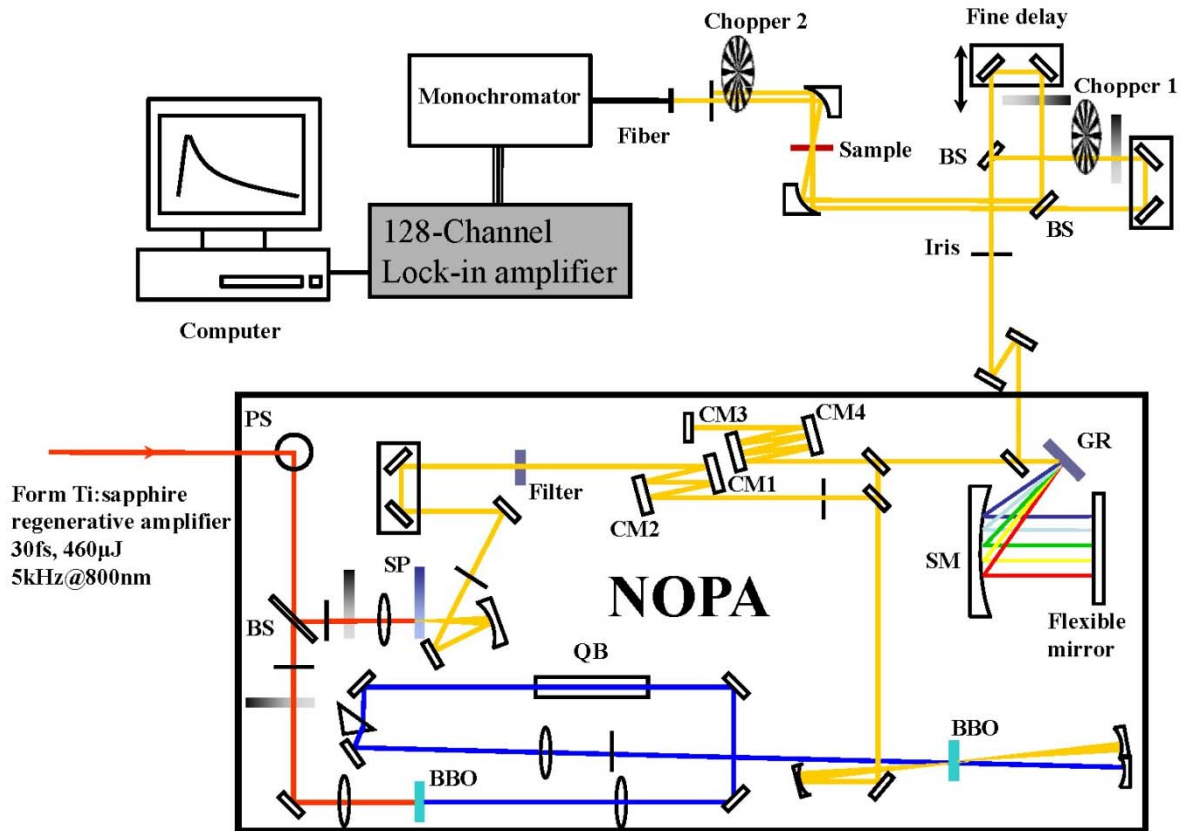
Figure 3-4 Schematic diagram of the visible sub-10 fs NOPA system and pump-probe experimental setup. PD: photodiode; BS: beam splitter; SP: sapphire plate; SM: spherical mirror; CM: ultrabroad-band chirped mirror; GR: 300-lines/mm ruled diffraction grating; QB: 10-cm quartz block; PS: periscope; VND: variable neutral-density filter.

in duration and covered the spectral range of 514-758 nm. Within the pulses, the spectral phase is almost constant resulting in nearly the Fourier-tansform limited pulses. The pump beam was mechanically chopped at 2.5 kHz in synchronization with the laser pulses at 5 KHz. The pump and probe beams were set collinear and focused on the samples. Then the probe beam intensity was synchronously detected by a Si photodiode attached to a monochromator (Prinston Instruments, SpectraPro 2300i). The intensity changes of transmitted probe beam induced by the pump were processed through a 128 channel lock-in amplifier referenced to the frequency and phase of chopper in pump beam.

## 3.3 Experimental detail

In this study, we performed both the shorter time region and the longer time region pump-probe experiments. The delay-time ranges were set between -300 fs and 1400 fs and between -0.9 ps and 14.5 ps, respectively. There are 500 data point in time region and 96 data points in the spectral range between 514 nm and 758 nm in each experimental data, and step width was 3.6 fs in the shorter time region experiment and 31 fs in the longer time region experiment. For these experiments, the full width at half maximum (FWHM) of the pulse was determined by second-harmonic generation frequency-resolved optical gating (SHG-FROG) measurements [40, 41] to be slightly shorter than 10 fs, within which it carried a nearly constant spectral phase. The pulse energies of the pump and probe were about 8 nJ and 0.8 nJ, respectively.

During the measurements, a liquid DR19 sample was taken in a 1-mm-thick quartz flow cell (Starna, Type : 48-Q-1) , and rapidly recirculated with a peristaltic pump through a 4 mm i.d. Tygon tube (R3603) to ensure the fresh sample after each laser shot. The configuration of circulation system was shown in Figure 3-5 (a). Large volumes of the liquid samples with 60 ml were chosen to avoid accumulation of photo-generated cis isomer. For the experiment of polymer films, the samples were placed on the holder which was connected with a vertical stage as shown in Figure 3-5 (b). The measured position of a film was varied after every measurement to avoid the damage on the surface caused by laser pulses. In case of the polymer films, the effect of accumulation may be considerable (The cis isomer thermally reforms the trans isomer with a time constant of several seconds or milliseconds) [42]. All the experiments were performed at room temperature.
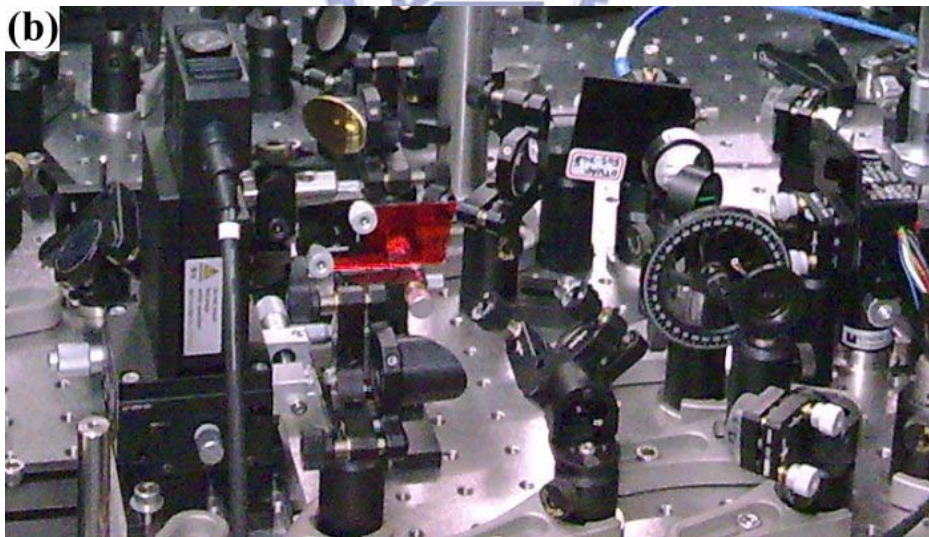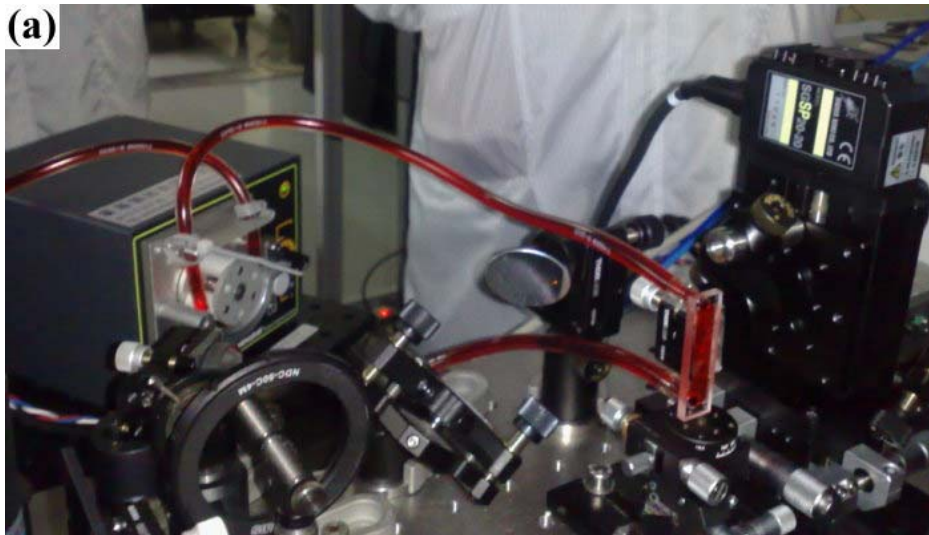
Figure 3-5 The photograph of the measurements for (a) a liquid sample and (b) a polymer film.

# Chapter 4

# Results and discussion

## 4.1 Femtosecond absorption spectroscopy in the shorter time region (from -300 fs to 1400 fs)

### 4.1.1 2D absorbance changes

The experimental data were represented with a two-dimensional (2D) plot of the transmittance changes ($\Delta T/T$) as a function of both the probe frequency and delay time. According to the calculating formula $\Delta A = -\log\left(1 + \frac{\Delta T}{T}\right)$, one can obtain the absorbance changes. Figure 4-1 shows the two-dimensional view of absorbance change spectrum, which has 500 data points in time region between -300 fs and 1400 fs with the interval of 3.6 fs and 96 data points in spectral region between 514 nm and 758 nm. The contour line of $\Delta A = 0$ is shown as black line. The photo induced absorbance changes $\Delta A$ for solution samples is negative in a spectral range of 514 nm to 578 nm and positive beyond this spectral range. Additionaly, the negative $\Delta A$ for polymer films is in a spectral range of 514 nm to 591 nm. The negative $\Delta A$ is caused by the absorption bleaching, which means the population of electrons depleted when DR19 was photoexcited by pump pulses. The positive $\Delta A$ is a result of the induced absorption of the excited state. The intense signal of $\Delta A$ near zero-delay time is attributed to a coherent spike, and the interference due to the superimposition of pump pulses and probe pulses is various at different wavelengths. Figure 4-2 and 4-3 show the $\Delta A$ as a function of delay time of DR19 in solution and a polymer film, respectively, for probe wavelengths of 558 nm, 583 nm, 609 nm, 635 nm, 660 nm, 686 nm, and 712 nm. The
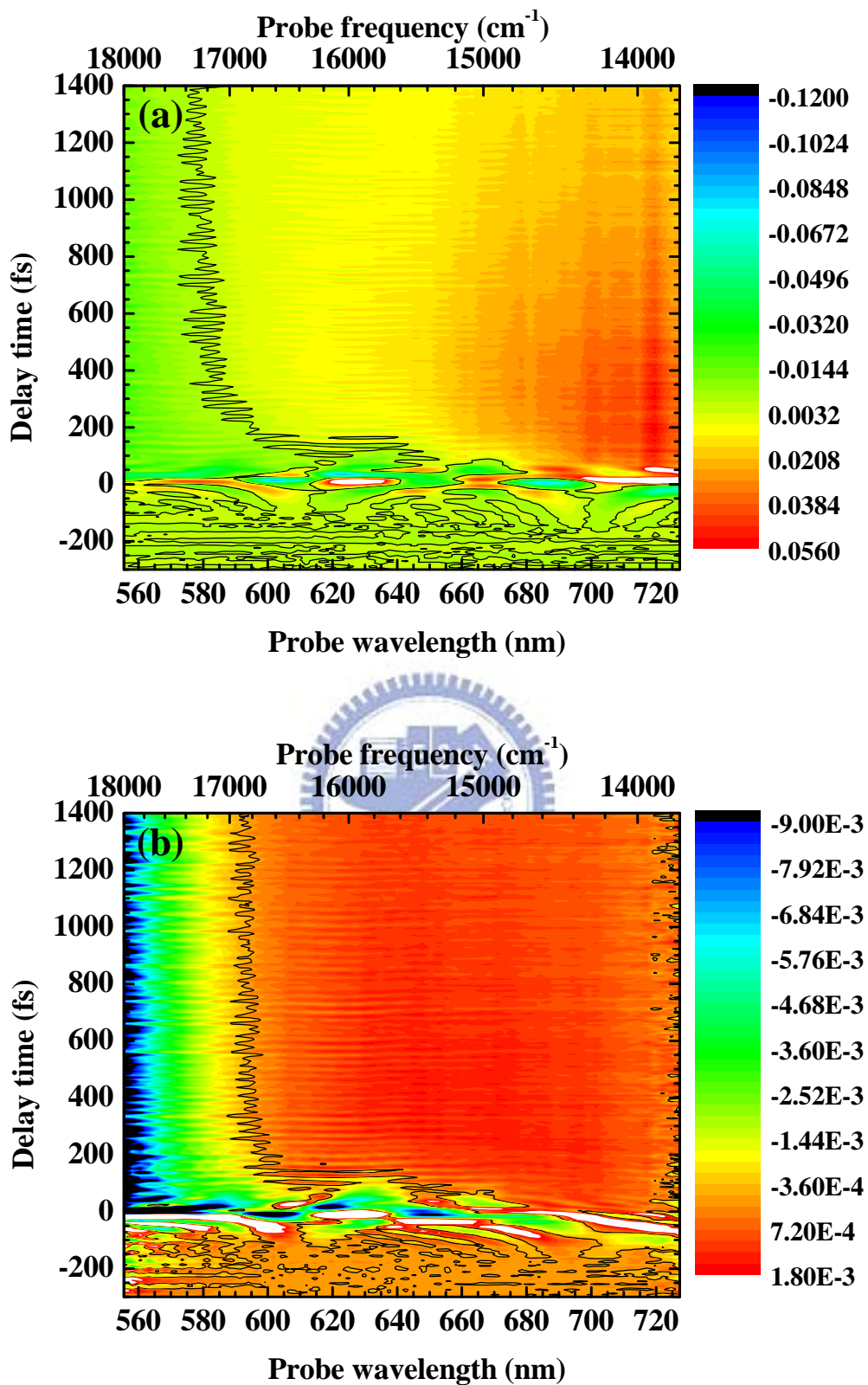
Figure 4-1 2D transient absorbance change spectrum of DR19 in (a) solution and (b) a polymer film.
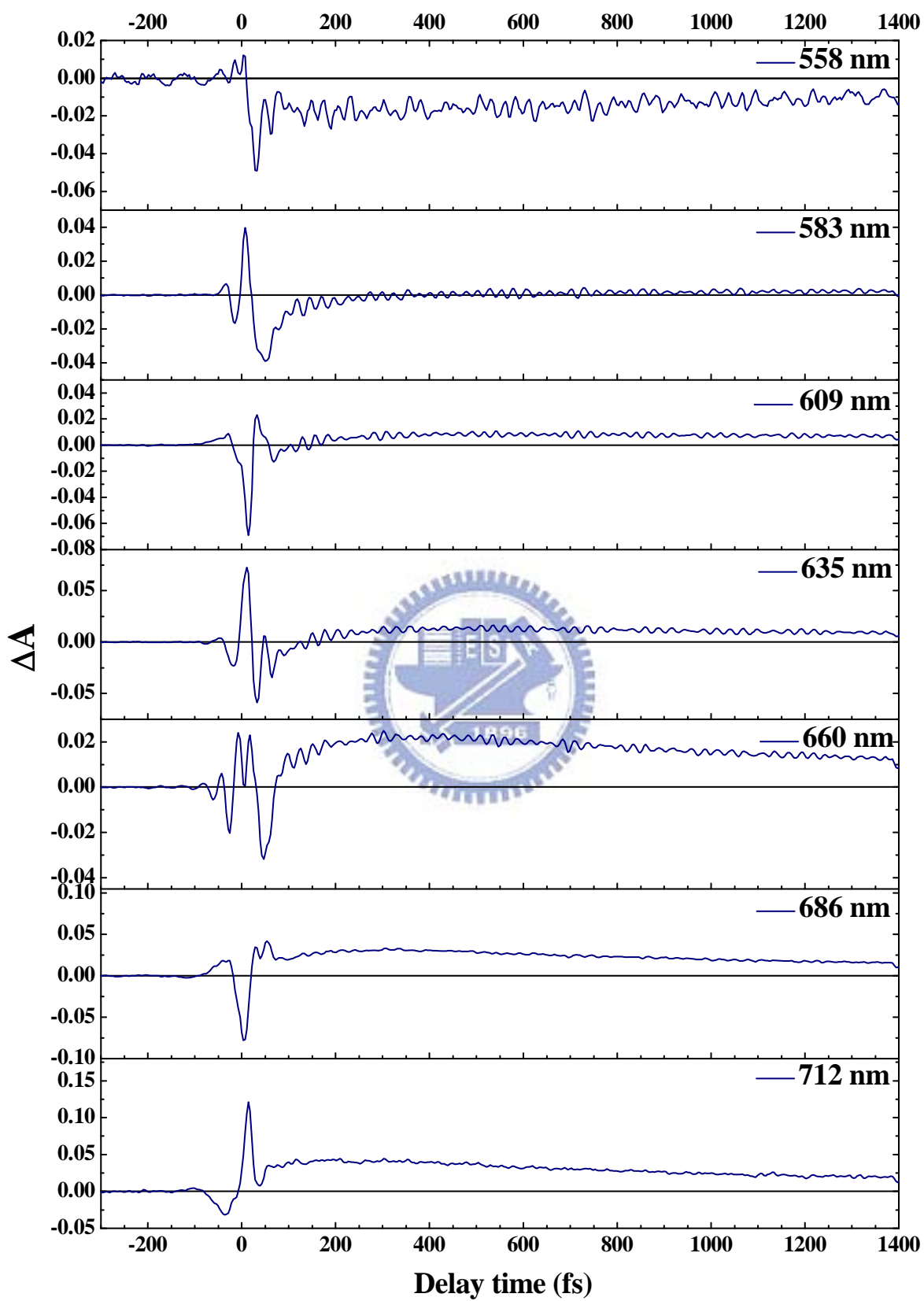
Figure 4-2 Transient absorbance changes of DR19 in solution at various probe wavelengths.
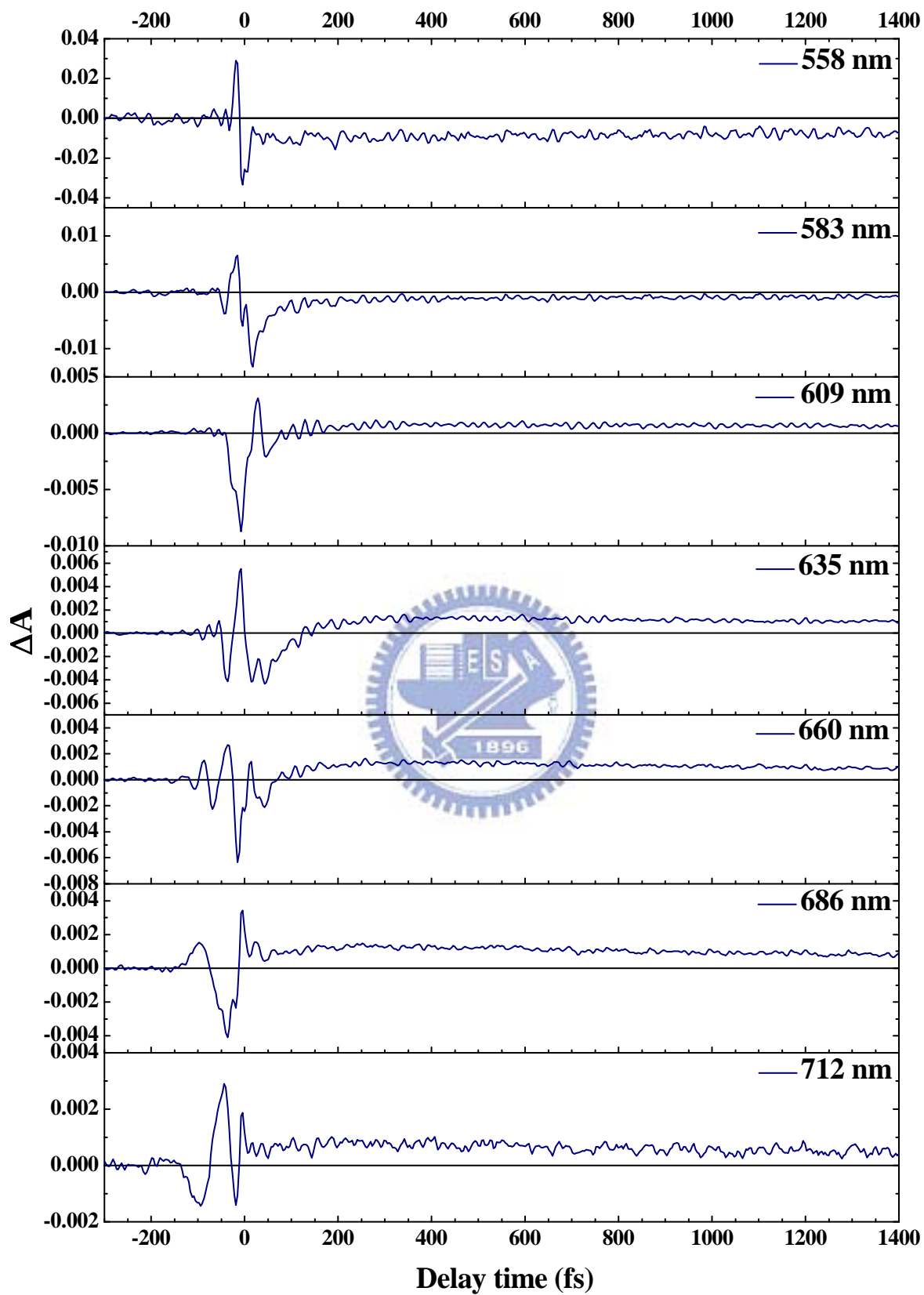
Figure 4-3 Transient absorbance changes of DR19 in a polymer film at various probe wavelengths.

negative photoinduced absorbance changes found at probe wavelength 558 nm are attributed to the bleaching of the ground state population. The absorbance changes is close to zero at 583 nm, where is neither bleaching nor photoinduced absorption. At the other probed wavelengths, the positive sign of $\Delta A$ is caused by the induced absorption of the excited state. The photoinduced absorbance changes exist up to 1400 fs due to the lifetime longer than the measured time region. These signals are composed of a slow relaxation dynamics and a periodical oscillation. The former is assigned to the electronic relaxation, and the latter is attributed to molecular vibration. The oscillatory signals exist up to 1400 fs after excitation, and they seem to be composed of two dominate frequencies. The Fourier transform of the periodical oscillation will reveal information about the vibrational amplitude and phase.

### 4.1.2 Lifetime fitting

The time-dependent absorbance changes is analyzed by the double-exponential decay fitting. Figure 4-4 shows the lifetime at all probed wavelengths. In these results with short scanning range in delay time, the longer lifetime cannot be fitted well and it will be discussed in subsection 4.2.2. However, the fast decay with a time constant of ~100 fs was observed in both samples. It has been attributed to a large amplitude motion of the excited molecule out of the Franck-Condon region [43]. Additionally, this attribution of the rapid internal conversion from the $S_2$ state to the $S_1$ state is also proposed in previous works by other groups [44, 45]. These experimental results indicate that the fast dynamic behavior in solution samples is similar to that in the polymer films.
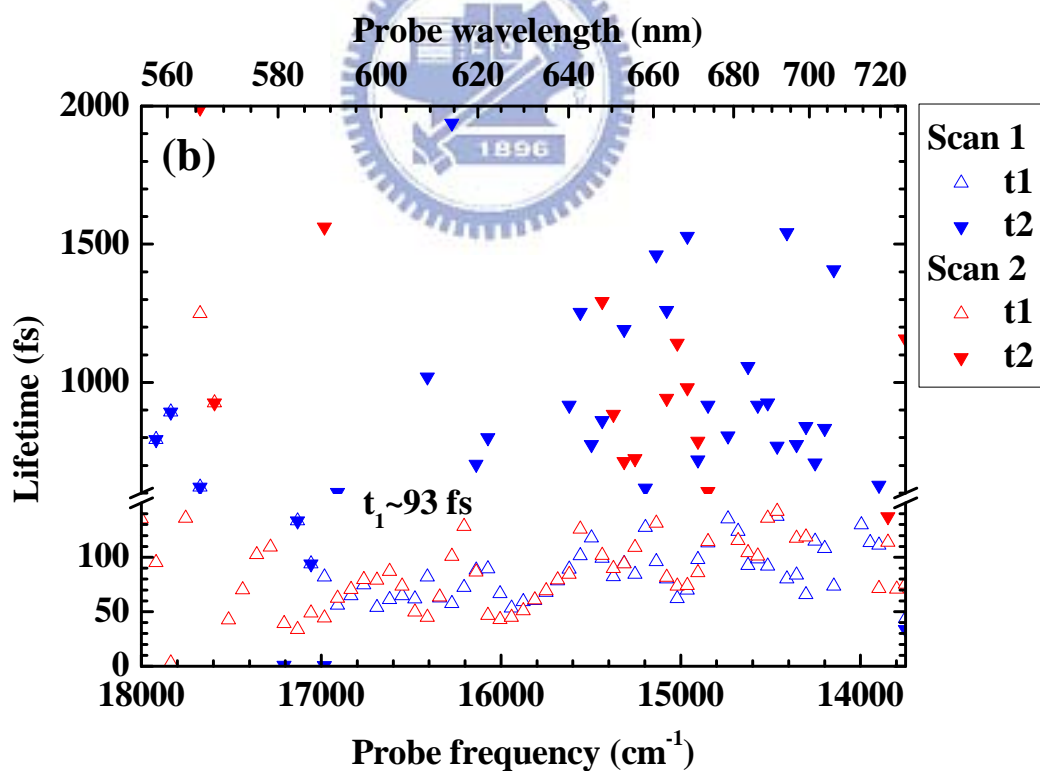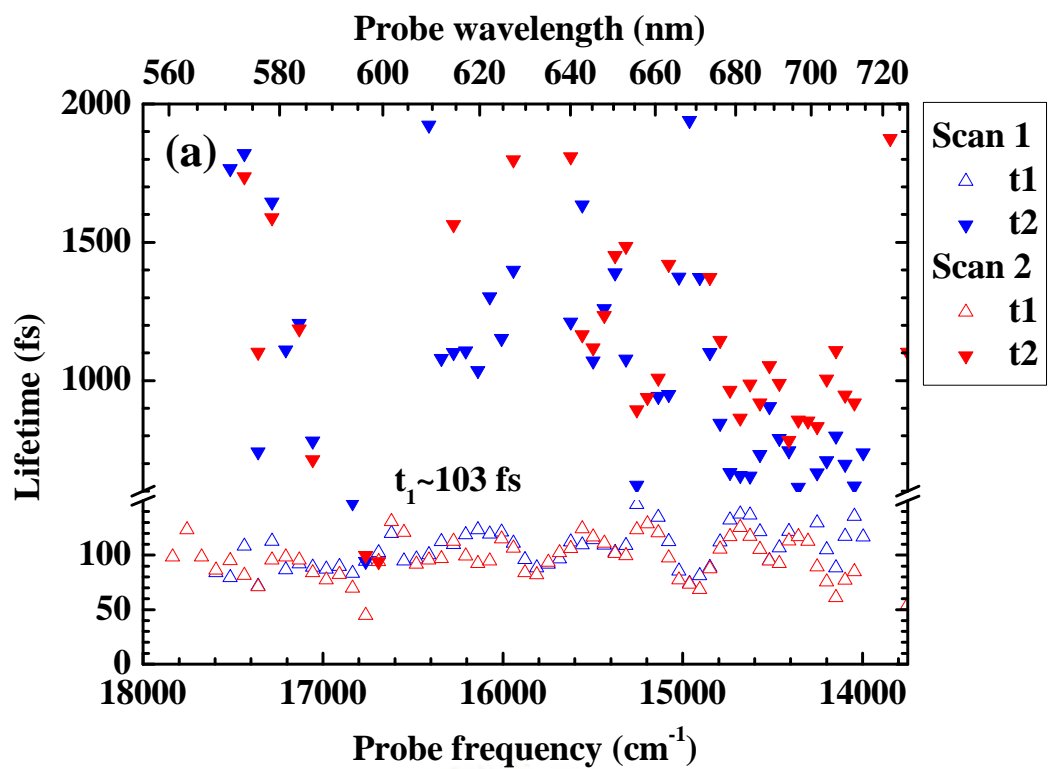
Figure 4-4 Lifetime of DR19 in (a) solution and (b) a polymer film.

### 4.1.3 Fast Fourier transform of the absorbance changes

With a multi-channel lock-in amplifier, the time-dependent absorbance changes were taken over the spectral range from 514 nm to 578 nm. The Fourier power spectra of oscillating components were obtained from the real-time trace by fast Fourier transform (integrated over the time range from 100 fs to 1400 fs since there are interference signals caused by the probe pulses and scattered pump pulses in the delay time earlier than 100 fs). The two-dimension plots of FFT power as a function of the molecular vibrational frequencies and probe wavelengths are shown in Figure 4-5. Several vibrational modes appear in FFT power spectrum, especially two prominent modes around 1105 $cm^{-1}$ and 1320 $cm^{-1}$. These modes may be expressed as the modes mixing due to the small difference in frequency between the adjacent modes, assigned to the stretching of C-C and symmetric stretching of $NO_2$, respectively. Both signals are also observed in the stationary Raman spectrum, e.g. Figure 2-5.

Figure 4-6 and 4-7 show the Fourier amplitude spectrum of real-time traces for probe wavelengths of 555 nm, 573 nm, 591 nm, 609 nm, 627 nm, 645 nm, 663 nm, and 681 nm. The intense peaks in the spectrum of a solution sample located around 470 $cm^{-1}$, 1105 $cm^{-1}$, 1180 $cm^{-1}$, 1320 $cm^{-1}$, and 1560 $cm^{-1}$ which are also observed in a polymer film (shown in Fig. 4-7) except for the 470 $cm^{-1}$ attributed to the solvent molecule of TMTE. In the FFT amplitude spectra, the dominant modes at 1105 $cm^{-1}$ and 1320 $cm^{-1}$ is strong probe wavelength dependence, and the FFT amplitude of peak in 1105 $cm^{-1}$ is drastically reduced at 591 nm in the solution case. The peak at 1180 $cm^{-1}$ assigned to the C-C stretching and coupled to C-N stretching is more intense in the solid state. For the pump-probe measurements, solutions of DR19 were recirculated with a peristaltic pump, and the pump-driven flow system was used to ensure that the laser pulses encountered fresh sample. However, the pulses were focused on the fixed point of a film, and the samples may have been damaged during the pump-probe
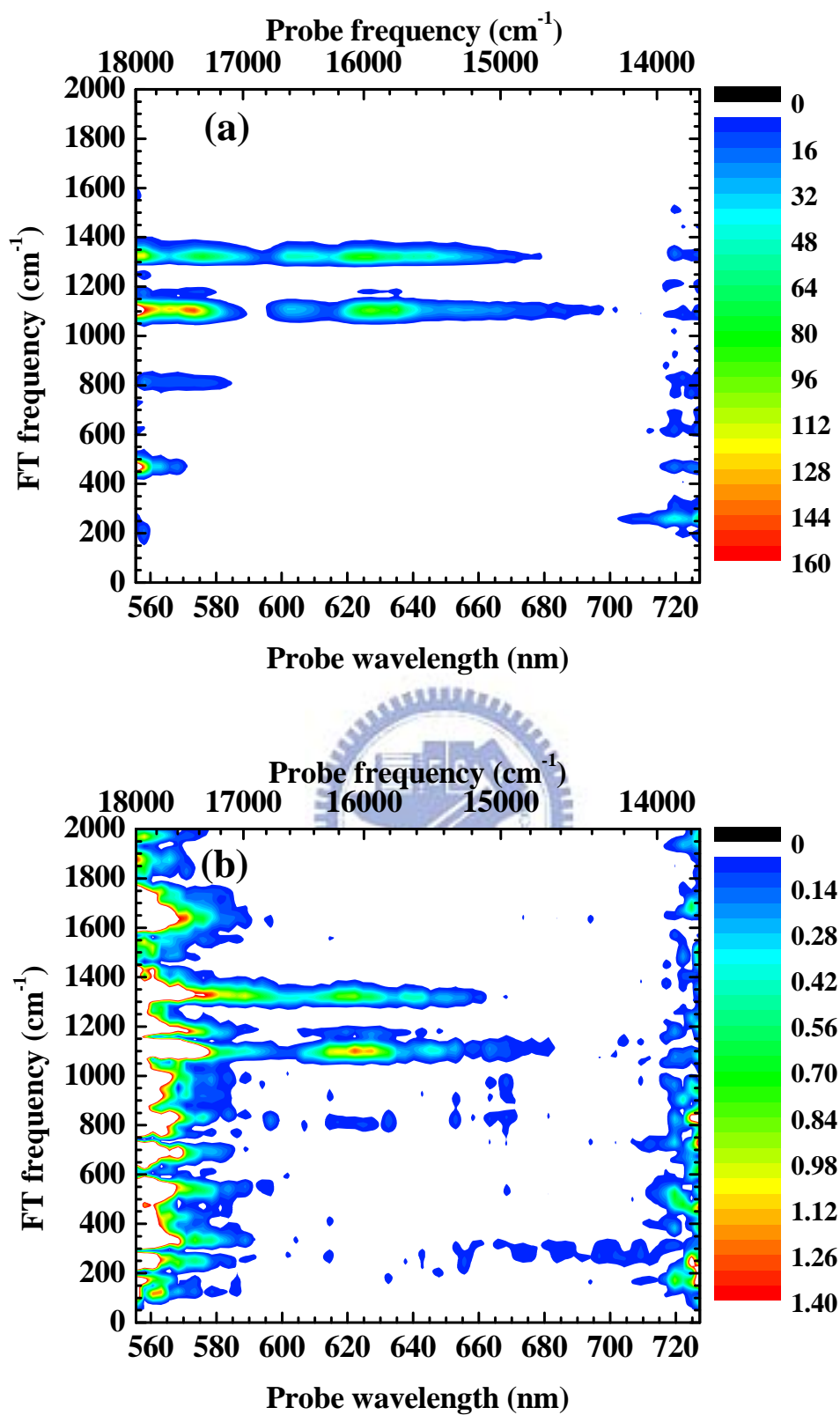
Figure 4-5 FFT power spectrum of vibration in the absorbance changes. DR19 in (a) solution and (b) a polymer film.
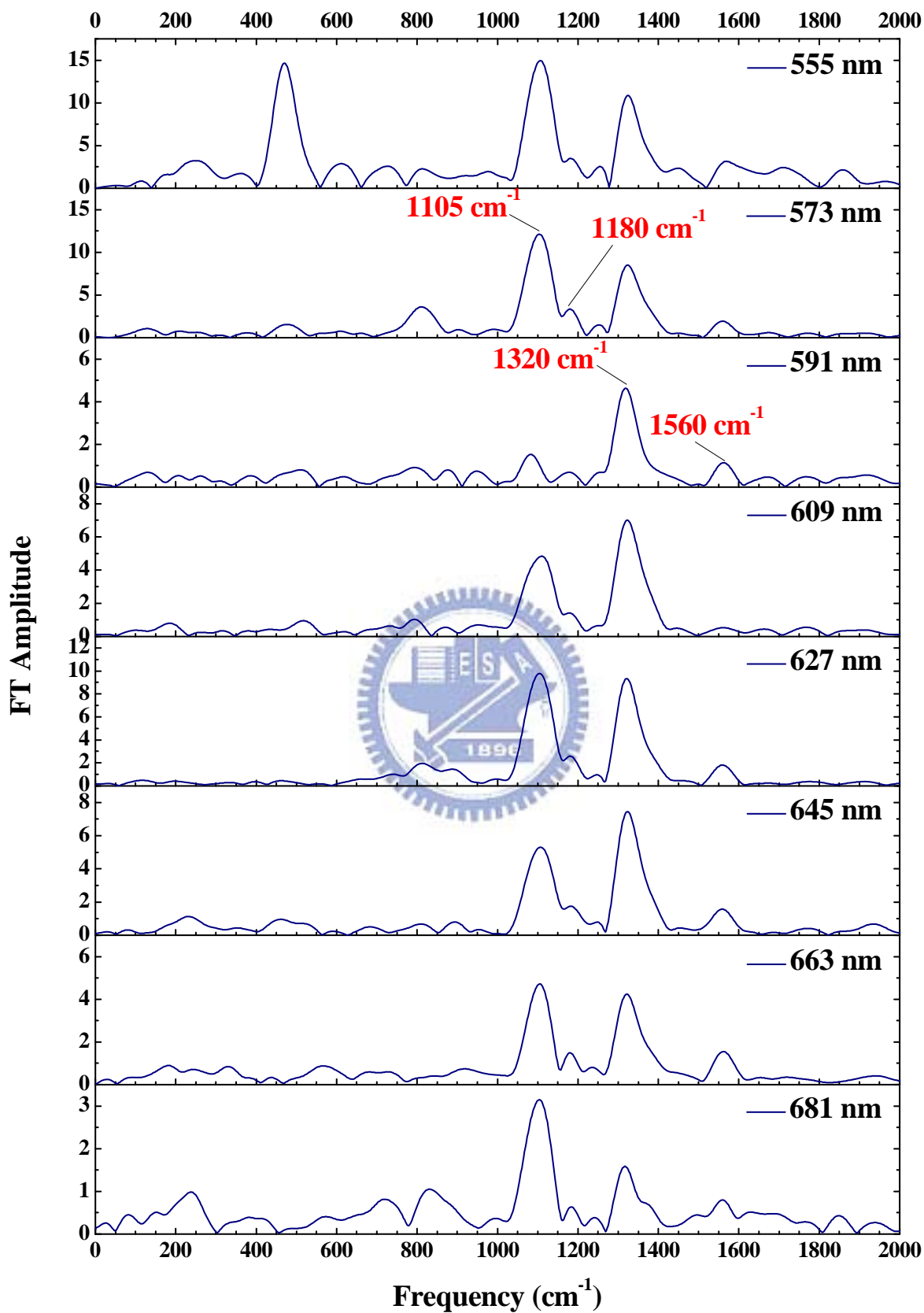
Figure 4-6 FFT amplitude spectra of DR19 in solution.
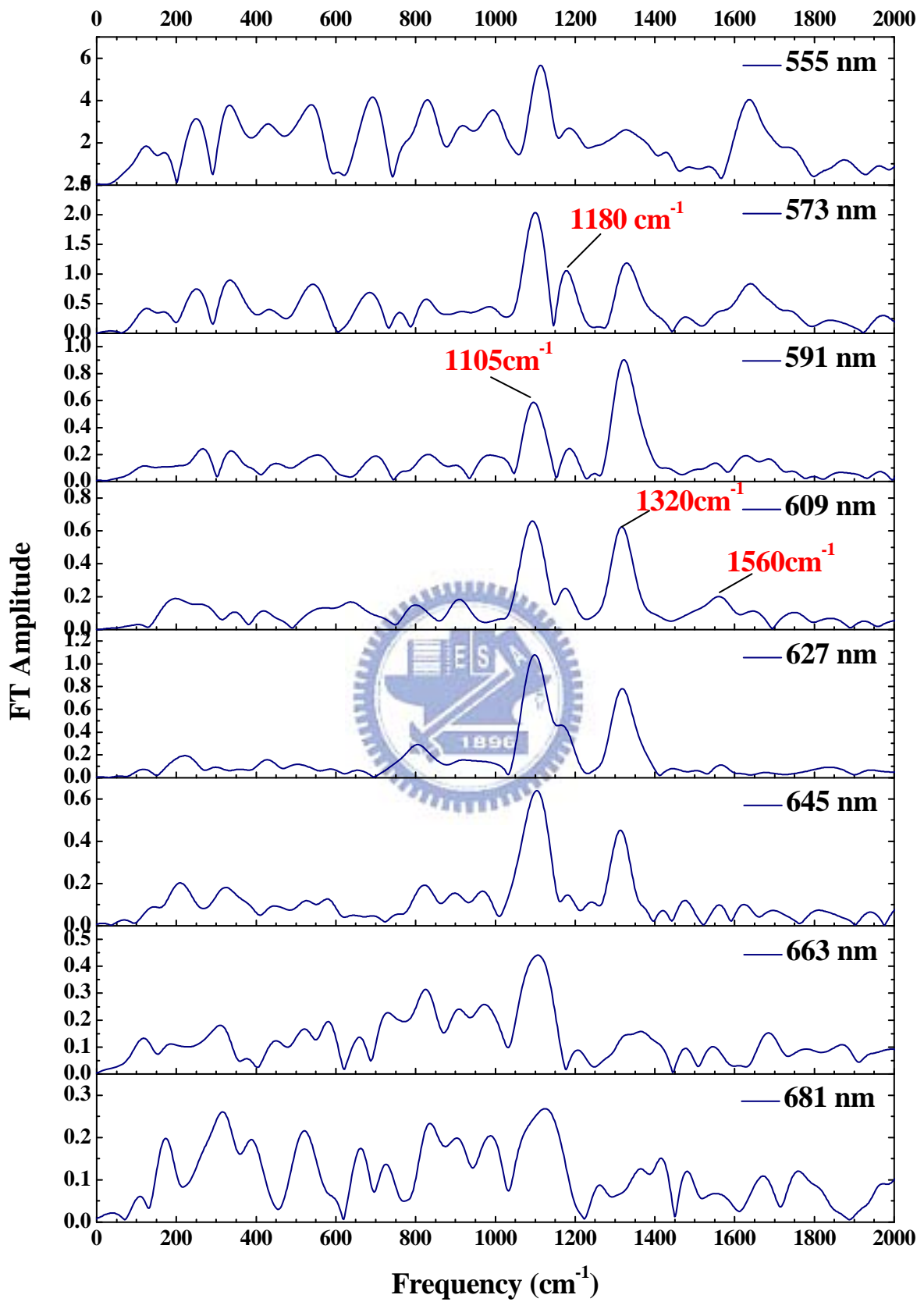
Figure 4-7 FFT amplitude spectra of DR19 in a polymer film.

measurements. For this reason, the absorbance changes in solution samples are larger than that in the polymer films, and the corresponding Fourier amplitudes of molecular vibrations in solution is also larger than that in the polymer films.

### 4.1.4 Analysis of molecular vibrations

In order to investigate the mode frequencies and the phase of the wavepacket motion, the probe wavelength-dependent oscillation at ~1105 cm$^{-1}$ and ~1320 cm$^{-1}$ were analyzed by the integration of FFT power with the band width 100 cm$^{-1}$, tracking the peak position, and the phase variations of the wavepacket motion in whole spectral range. The analytic results of 1105 cm$^{-1}$ and 1320 cm$^{-1}$ are shown in Figure 4-8 and 4-9, respectively. The FFT power of the C-C stretching (1105 cm$^{-1}$) clearly exhibit intense band in the spectral range of 550 nm to 580
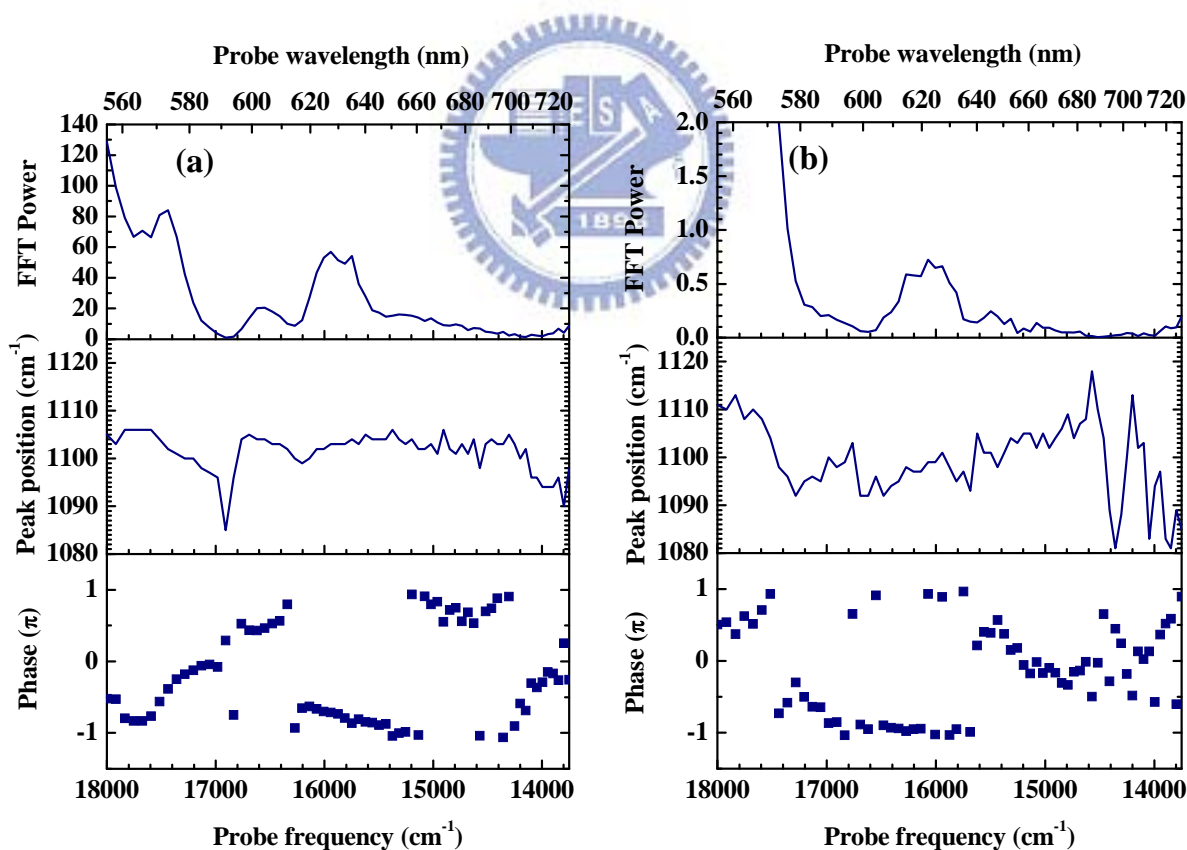


Figure 4-8 Reproducible peak tracking of molecular vibration at 1105 cm$^{-1}$ in (a) solution and (b) a polymer film.
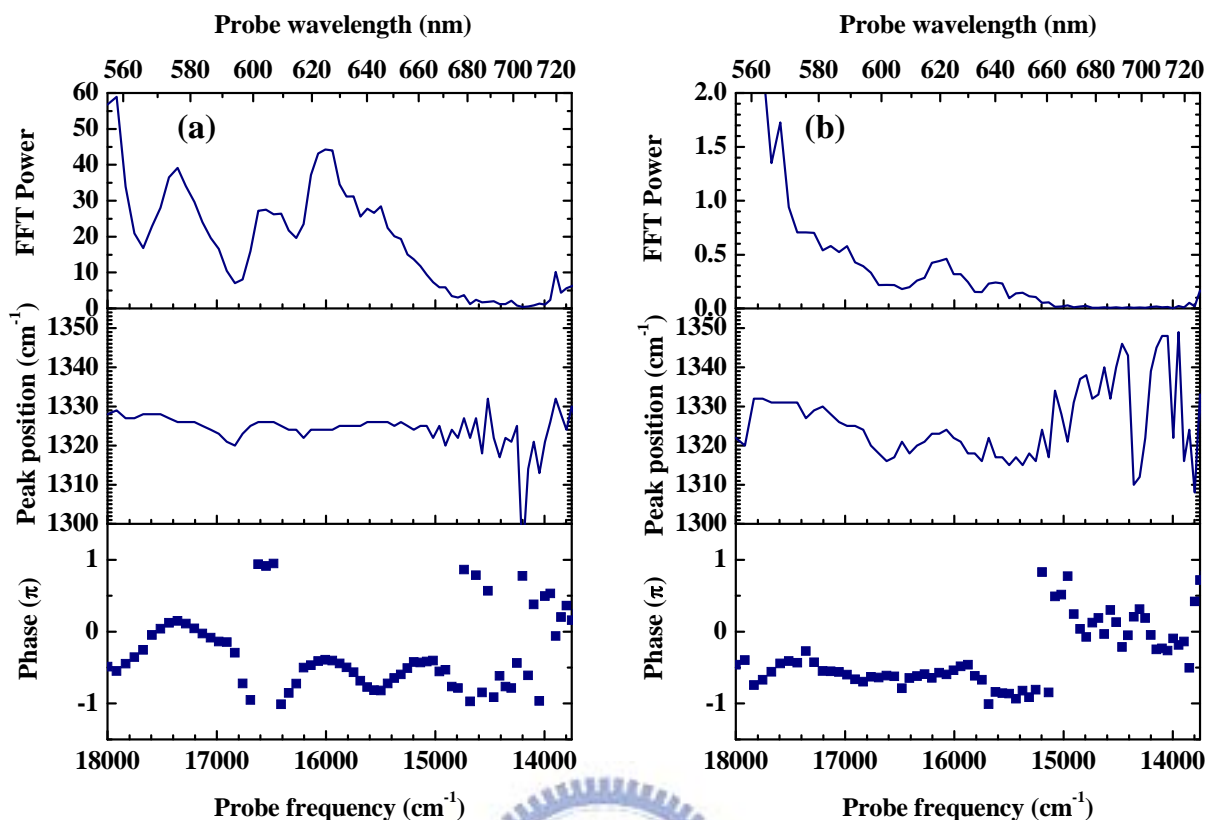
Figure 4-9 Reproducible peak tracking of molecular vibration at 1320 cm$^{-1}$ in (a) solution and (b) a polymer film.

nm and 615 nm to 645 nm. The peak position of the C-C stretching almost keep constant with 1105 cm$^{-1}$ in whole spectral range, as shown in Figure 4-8. Additionally, the phase is around zero, -$\pi$ or $\pi$ in both samples, which corresponds to a wavepacket motion in the excited state. The probe wavelength-dependent FFT power of the NO$_2$ symmetric stretching (1320 cm$^{-1}$) shown in Figure 4-9 are similar to the FFT power of the C-C stretching (1105 cm$^{-1}$). The peak position of the NO$_2$ symmetric stretching are around 1320 cm$^{-1}$ for both samples in solution and a polymer film. However, the phase of wavepacket motion seems be modulated by the frequency of ~900 cm$^{-1}$ in solution samples, which is absent in a polymer film.

## 4.2 Femtosecond absorption spectroscopy in the longer time region (from -0.9 ps to 14.5 ps)

### 4.2.1 2D absorbance changes

Since the isomerization proceeds of azo dye with a time constant is greater than 2 ps, it is hard to determine the electronic relaxation time of isomerization of azo dye within the shorter delay-time range. So the pump-probe experiments with longer delay time were also performed in this study. Figure 4-10 shows the two-dimensional view of absorbance change spectrum, which has 500 data points in time region between -0.9 ps and 14.5 ps with the interval of 31 fs and 96 data points in spectral region between 514 nm and 758 nm. Black lines represent the contour line of $\Delta A = 0$. In the longer wavelength range (from 640 nm to 720 nm), the intense absorbance changes of DR19 in solution is positive and decay within 3 ps. However, in the spectral range between 590 nm and 640 nm, the decay is not clearly observed and the relaxtion dynamics is different from that in longer wavelength range from 640 nm to 720 nm. Moreover, this significant characteristics of DR19 in solution are obviously smeared out in the spectrum of DR19 in a polymer film as shown in Fig. 4-10(b).

Figure 4-11 and 4-12 show the transient absorbance changes at various probe wavelengths. Due to the scanning step with 31 fs is larger than the oscillation periods of molecular vibrations, the periodical component is absent in the transient absorbance change spectrum. The positive photoinduced absorbance changes are clearly observed in both cases of solution and a polymer film. However, the negative $\Delta A$ only appear arround 558 nm in a polymer film. The further analysis of the transient absorbance changes will be shown in next two subsections.
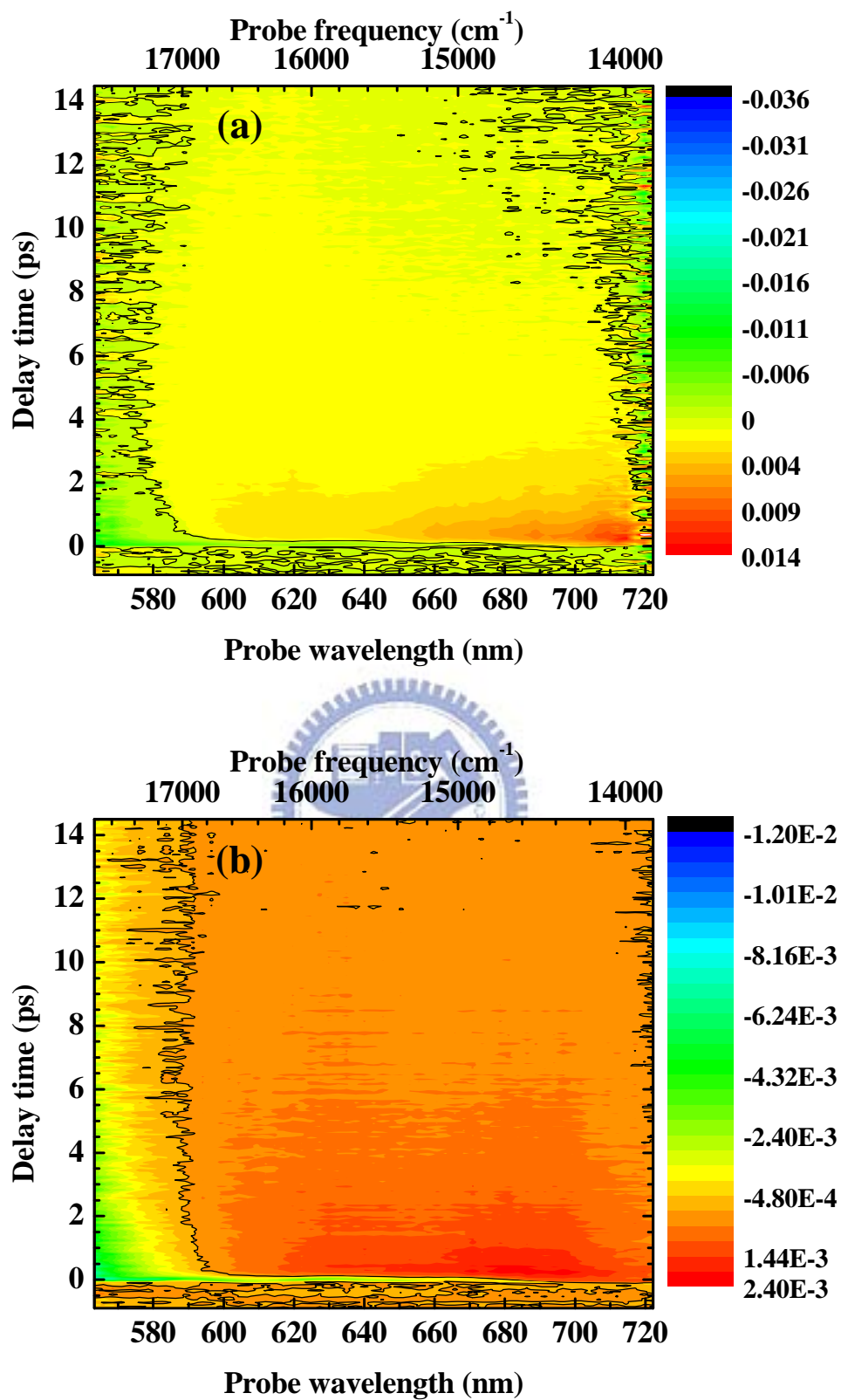
Figure 4-10 2D transient absorbance change spectrum of DR19 in (a) solution and (b) a polymer film.
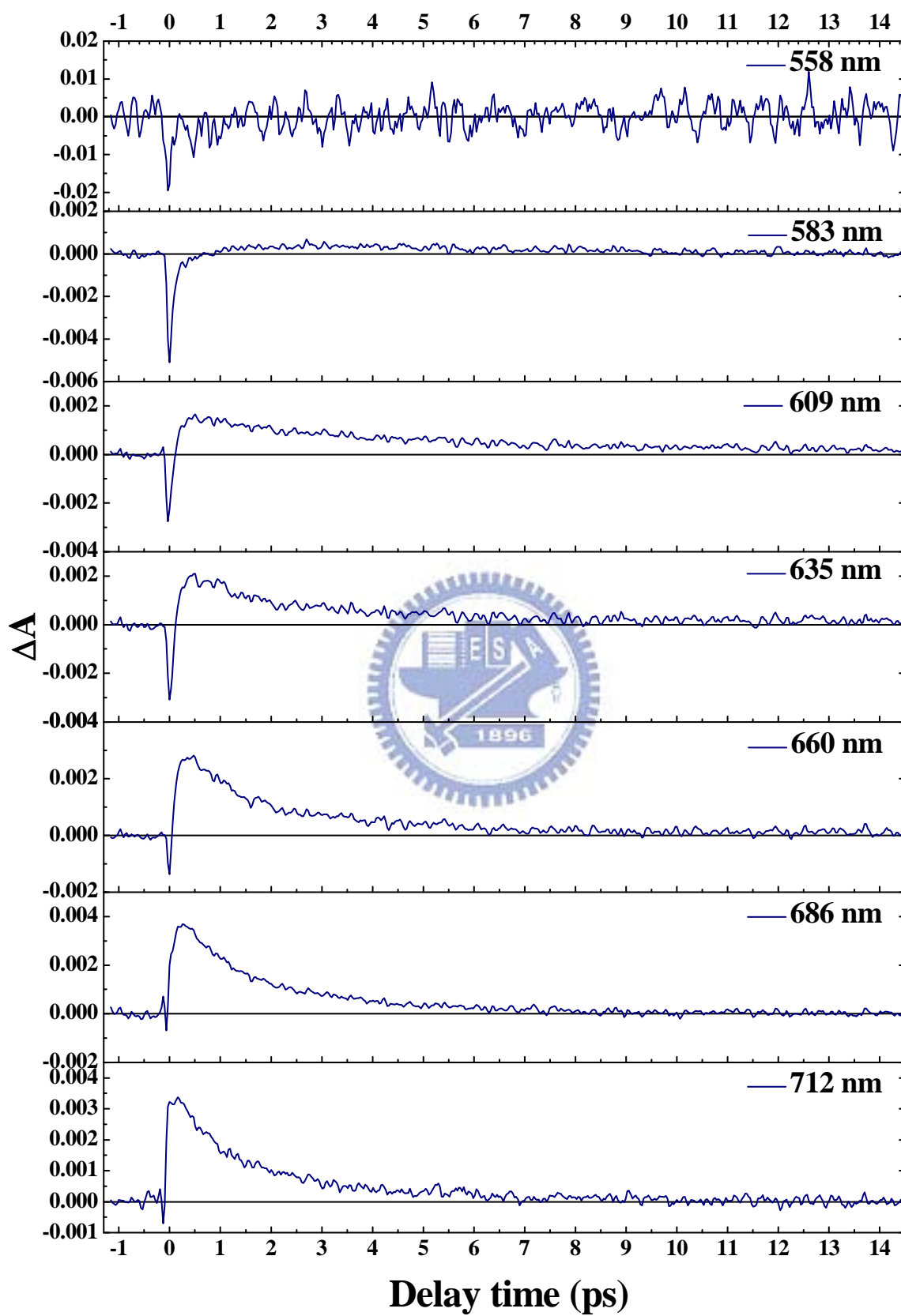
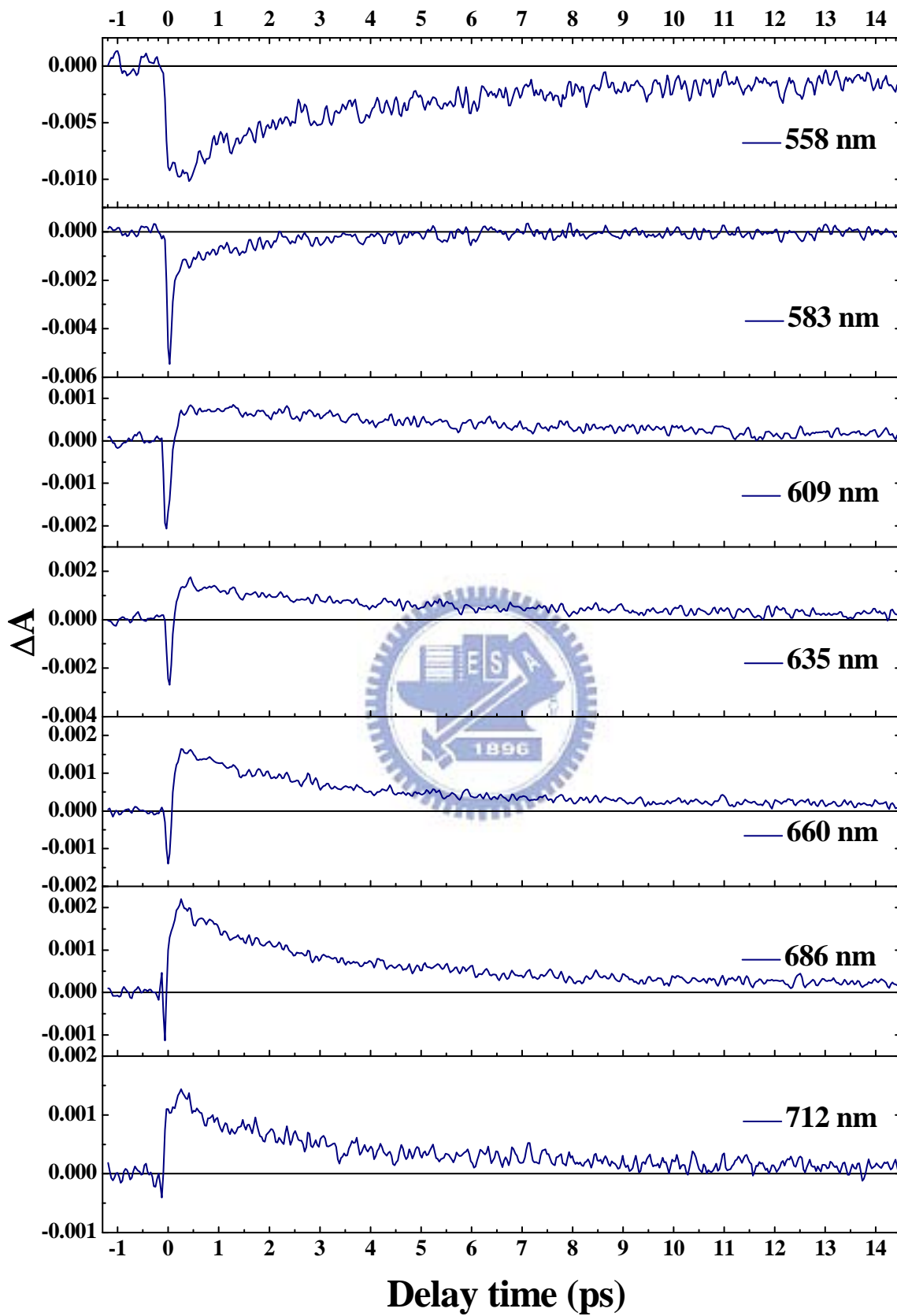Figure 4-11 Transient absorbance changes of DR19 in solution at various probe wavelengths.

Figure 4-12 Transient absorbance changes of DR19 in a polymer film at various probe wavelengths.

**4.2.2 Time-resolved spectrum**

The transient absorption spectra at various delay time are shown in Figure 4-13 and 4-14. In order to obtain the smoother curve, the data points adjoined delays (±0.5 ps) were averaged to be one data point of absorbance change in each delay time. As shown in Figure 4-13, in the range of longer wavelengths between 640 nm and 710 nm, the absorbance changes decrease dramatically in the delay time earlier than 2 ps, and decrease slowly in the later delay times. The rapid decay is caused by the photoinduced absorption in the excited state, but the decay is slow in the spectral range between 595 nm and 640 nm. In the range of shorter wavelengths between 555 nm and 580 nm, the ΔA increased with time and the bleaching band does not return to zero during the measurements. The transient absorption spectra of DR19 in a polymer film are different from the results in solution, as shown in Figure 4-14. The absorbance changes decrease with similar rate in the range of wavelengths between 620 nm and 700 nm.
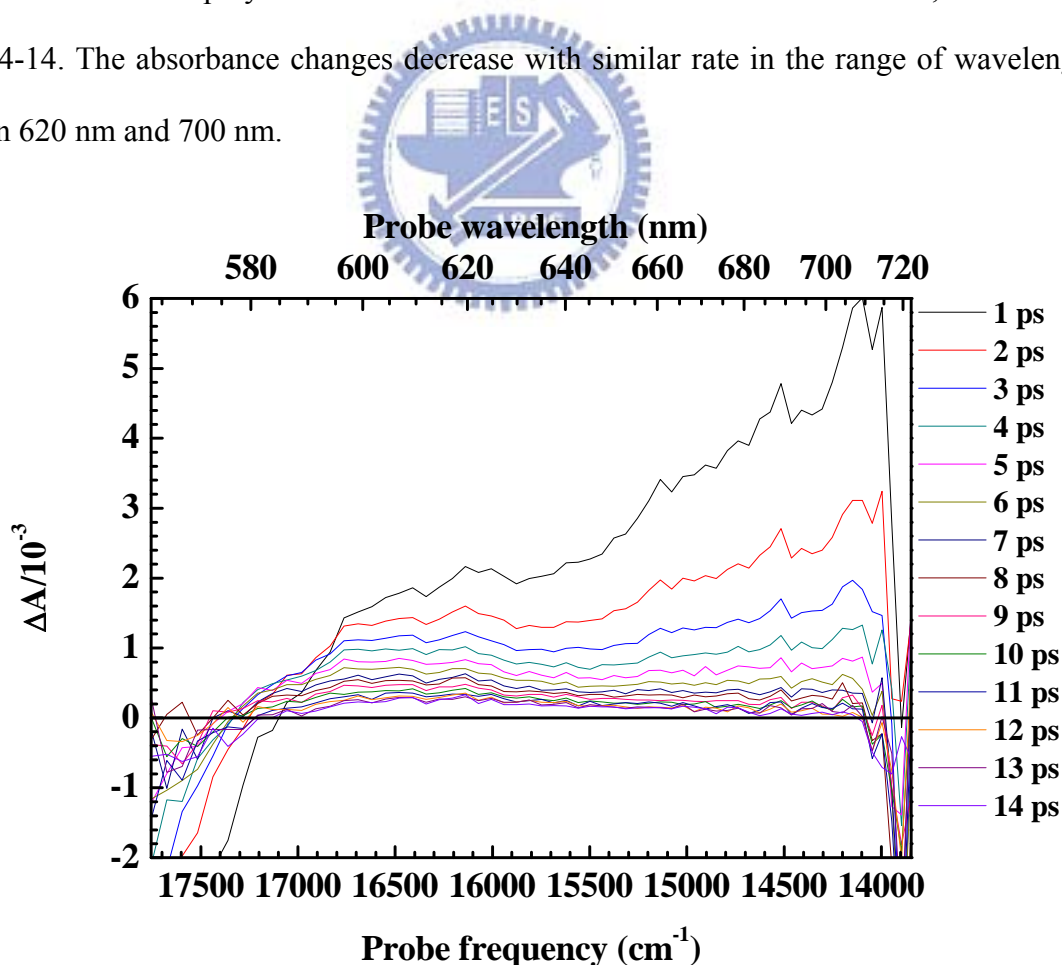


Figure 4-13 Transient absorption spectra at various delay time for DR19 in solution.
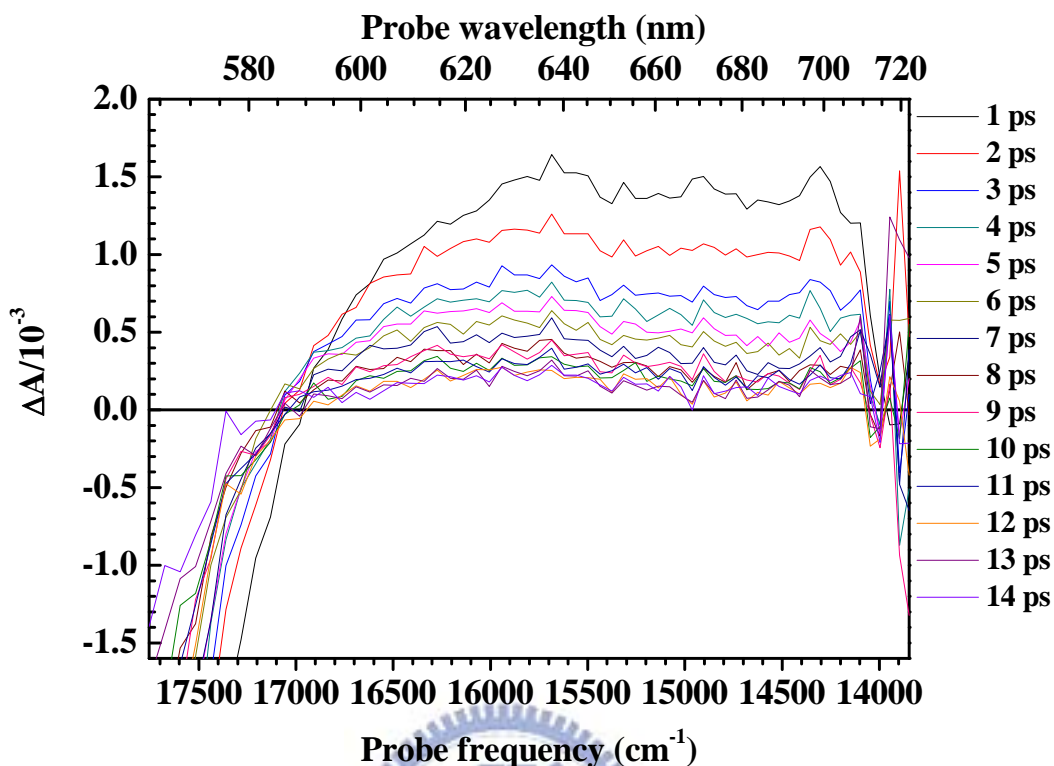
Figure 4-14 Transient absorption spectra at various delay time for DR19 in a polymer film.

### 4.2.3 Electronic relaxation time

The transient absorbance changes in longer time region were also analyzed by the double-exponential decay fitting. Figure 4-15(a) and (b) show the lifetime of DR19 in solution and a polymer film at all probed wavelengths, respectively. The relaxation time of ~0.63 ps and ~2.55 ps in solution between 640 nm and 700 nm were attributed to the internal conversion to the ground state and vibrational cooling in the ground state, respectively, which is consistent with the studies of Schmidt *et al*. in a push-pull substituted azobenzene (4-nitro-4'-(dimethylamino)azobenzene, NA) [43]. In solution as shown in Figure 4-15(a), the shorter time constant keeps in the same value ~ 0.63 ps in most spectral range while the longer time constant is wavelength-dependent in the range between 590 nm and 640 nm. For the case of DR19 in a polymer film as shown in Figure 4-15(b), both time
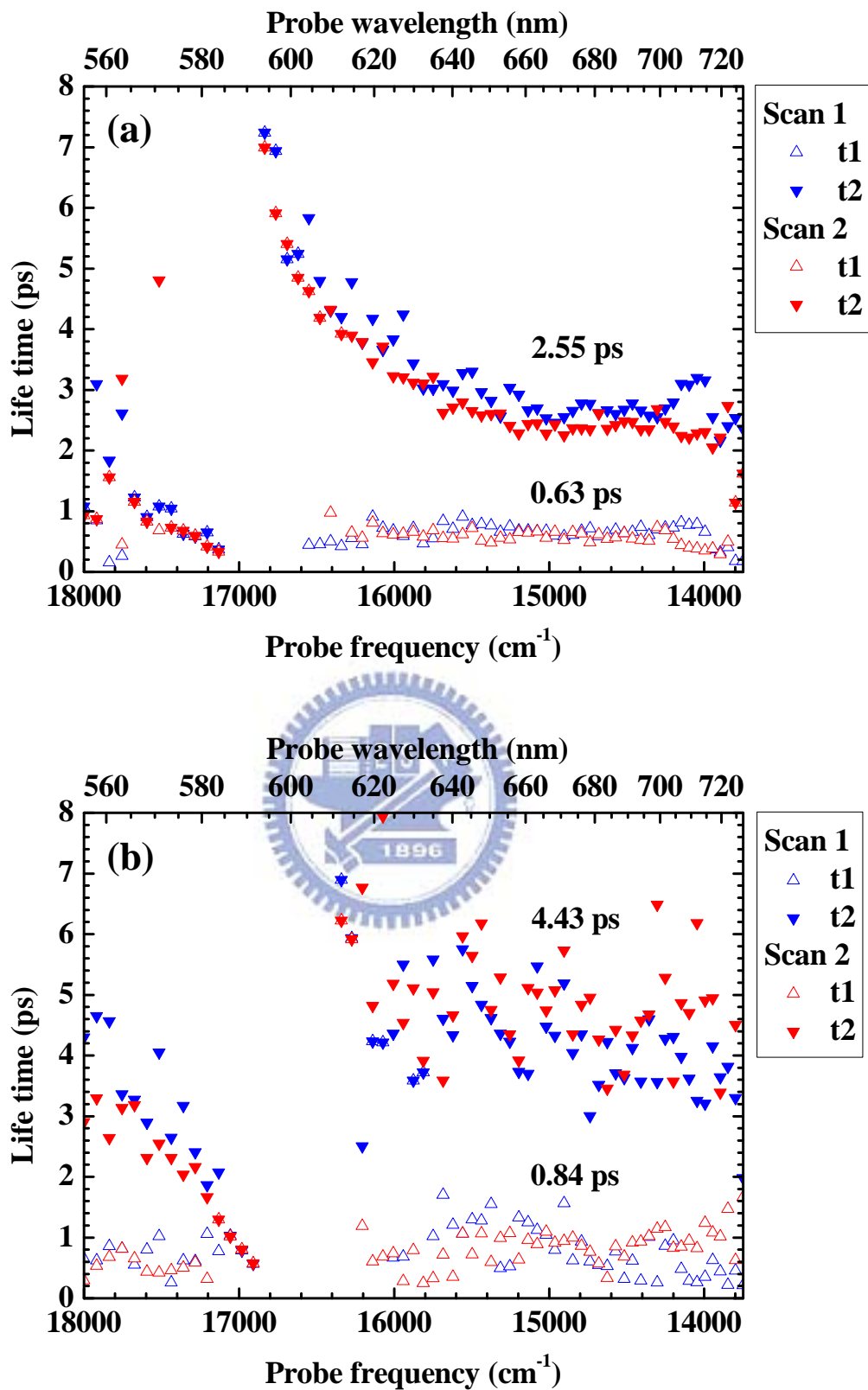
Figure 4-15 Lifetime of DR19 in (a) solution and (b) a polymer film.

constants (~0.84 ps and ~4.43 ps) seem to be wavelength–independent between 590 nm and 640 nm. All of the relaxation processes in the excited state vanished within 2.55 ps in solution and 4.33 ps in a polymer film. This implies that the isomerization dynamics of trans-DR19 are sensitive to the molecular environment. The relaxation process of trans-DR19 in solution and a polymer film is sketched in Figure 4-16. Namely, the trans-DR19 will be excited from $S_0$ ground state to $S_2$ excited state (Franck-Condon state), and then relax to $S_1$ state within ~100 fs (the black arrows in Figure 4-16). Due to the internal conversion, the trans-DR19 will relax to cis-DR19 or trans-DR19 with sub-ps (the red arrows in Figure 4-16). Finally, the cis-DR19 and trans-DR19 are, respectively, cooled from high-energy level to low-energy level of ground ($S_0$) state within several ps (the blue arrows in Figure 4-16).



Figure 4-16 Schematic diagram of the relaxation of trans-DR19 after photoexcitation in solution and a polymer film.

# Chapter 5
# Summary

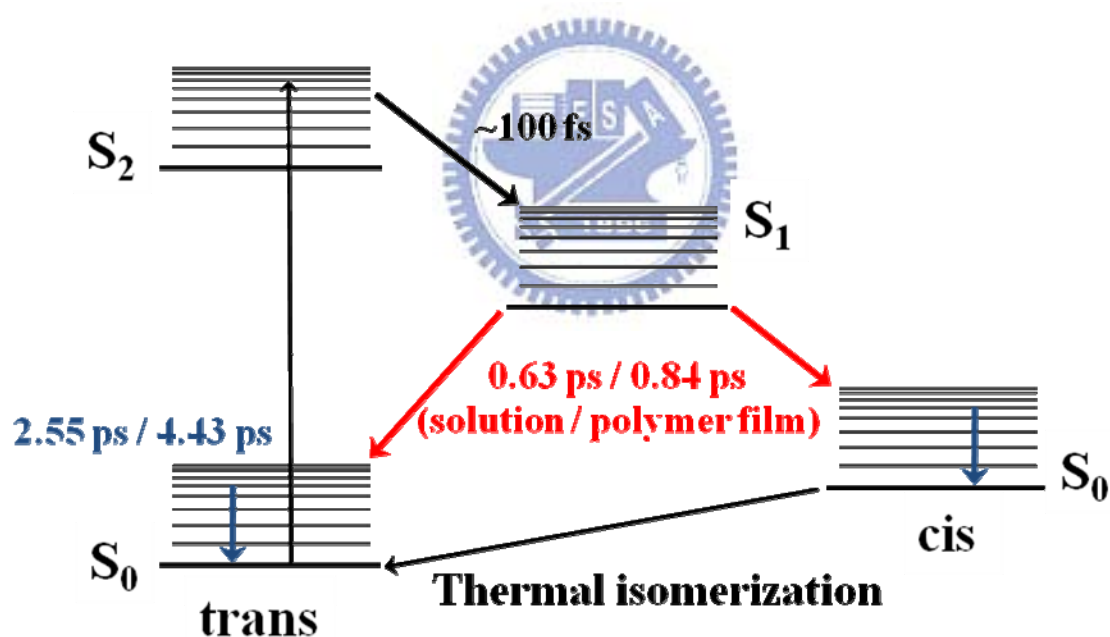The photoisomerization of DR19 in solution and a polymer film were investigated by sub-10 fs time-resolved absorption measurements with broadband visible spectral range. The most important results are described as follows,

(1) In the shorter time range, the motion of a wavepacket in the excited state out of the Franck-Condon state occurs on the time scale of ~100 fs in both samples with the form of solutions and films. The vibrational frequencies obtained from the FFT power spectra of solution samples are consistent with the vibrational frequencies in polymer films, but there are slightly difference in the wavepacket motion associated to the symmetric stretching of $NO_2$. These results indicate the molecular vibrations are not deeply influenced by the surrounding environment.

(2) In the longer time range, the internal conversion to the ground state processed with a time constant of ~0.63 ps in solution and ~ 0.84 ps in a polymer film. In addition, the longer time constant of ~2.55 ps in solution and ~4.43 ps in a polymer film are attributed to the vibrational cooling in the ground state.

These results suggest that the isomerization of DR19 is strongly influenced by the molecular environment. Furthermore, this study provides the essential information for photonics applications such as optical switches and optical memory storage devices, which put the photoisomerization mechanism in use.

# References

[1] Hartley, G. S. *Nature* 1937, 281; *J. Chem. Soc.* **1938**, 633-642

[2] Rau, H.; Lüddecke, E. *J. Am. Chem. Soc.* **1982**, 104, 1616

[3] Siampiringue, N.; Guyot, G.; Monti, S.; Bortolus, P. *J. Photochem.* **1987**, 37, 185

[4] Okamoto, H.; Hamaguchi, H.; Tasumi, M. *Chem. Phys. Lett.* **1986**, 130, 185

[5] Biancalana, A.; Campani, E.; Gorini, G.; Masetti, G.; Quaglia, M. *J. Raman Spectrosc.*
   **1992**, 23, 155

[6] Stuart, C. M.;Frontiera, R. R.; Mathies, R. A. *J. Phys. Chem. A* **2007**, 111, 12072-12080

[7] Curtis, R. D.; Hilborn, J. W.; Wu, G.; Lumsden, M. D.; Wasylishen, R. E.; Pincock, J. A. *J.*
*Phys. Chem.*, Int. Ed. Engl. **1993**, 97, 1856

[8] Armstrong, D. R.; Clarkson, J.; Smith, W. E. *J. Phys. Chem.* **1995**, 99, 17825

[9] Cembran, A.; Bernarli, F.; Garavelli, M.; Gagliardi, L.; Orlandi, G. *J. Am. Chem. Soc.*
   **2004**, 126, 3234

[10] Conti, I.; Garavelli, M.; Orlandi, G. *J. Am. Chem. Soc.* **2008**, 130, 5216

[11] Lednev, I. K.; Ye, T. Q.; Matousek, P.; Towrie, M.; Foggi, P.; Neuwhl, F. V. R.; Umapathy,
    S.; Hester, R. E.; Moore, J. N. *Chem.Phys. Lett*, **1998**, 290, 68

[12] Bortollus, P.; Monti, S. *J. Phys. Chem.* **1979**, 83, 648

[13] Rau, H. In *Photochromism: Molecular and Systems*; Dürr, H., Bouas-Lauran, H., Eds.;
    Elservier: Amsterdarn, **2003**; p 165

[14] Bortolus, P.; Monti, S. *J. Phys. Chem.* **1979**, 83,648

[15] Wildes, P. D.; Pacifici, J. G.; Gether, I. J.; Whitten, D. G. *J. Am. Chem. Soc.* **1971**, 93,
    2004

[16] Liu, Z. F.; Hashimoto, K.; Fujishima, A. *Nature* **1990**, 347, 658

[17] Sekkat, Z.; Dumont, M. *Appl. Phys. B* **1992**, 54, 486

[18] Ikeda, T.; Tsutsumi, O. *Science* **1995**, 268, 1873.

[19] Tamai, N.; Miyasaka, H. *Chemical Reviews* **2000**, 100, 1875-1890

[20] Jung, C. C.; rutloh, M.; Stumpe, J. ***J. Phys. Chem. B*** 2005, 109, 7865-7871

[21] Muraoka, T.; Kinbara, K.; Aida, T. ***Nature*** 2006, 440, 512-515

[22] Fujino, T.; Arzhantsev, S. Yu.; Tahara, T. *J. Phys. Chem. A* **2001**, 105, 8123

[23] Baltuska, A.; Fuji, T.; Kobayashi, T.; Opt. Lett. **2002**, 27, 306

[24] Chang, C. W.; Lu, Y.-C.; Wang, T.-T.; Diau, E. W.-G. *J. Am. Chem. Soc.* **2004**, 126, 3234

[25] Myers, A. B.; Mathies, R. A. *J. Chem. Phys.* **1984**, 81, 1552

[26] Sension, R. J.; Repinec, S. T.; Szarka, A. Z.; Hochstrasser, R. M. *J. Chem. Phys.* **1993**, 98, 6291 and references therein

[27] Polanyi, J. C.; Zewail, A. H.   *Acc. Chem. Res.* **1995**, 28, 119

[28] Lednev, I. K.; Ye, T. Q.; Hester, R. E.; Moore, J. N. *J. Phys. Chem.* **1996**, 100, 13338

[29] Asano, T.; Okada, T.; Shinkai, S.; Shigematsu, K.; Kusano, Y.; Manabe, O. *J. Am. Chem. Soc.* **1981**, 103, 5161

[30] Shin, D. M.; Whitten. D. G. *J. Am. Chem. Soc.* **1988**, 110, 5206

[31] Crecca, C. R.; Roitberg, A. E. J. Phys. Chem. A **2006**, 110, 8188

[32] Biswas, N.; Umapathy, S. *J. Phys. Chem. A* **2000**, 104, 2734

[33] Ando, R. A.; Rodriguez-Redondo, J. L.; Sastre-Santos, A.; Fernandez-Lazaro, F.; Azzellini, G. C.; Borin, A. C.; Santos, P. S. *J. Phys. Chem. A* **2007**, 111, 13452

[34] Clarkson, J.; Smith, W. E. *J. Mol. Struct.* **2003**, 655, 413

[35] Biswas, N.; Umapathy, S. *J. Raman Spectrosc.* **2001**, 32, 471

[36] Cerullo, G.; Manzoni, C.; Lüer, L; Polli, D. *Photochem. Photobiol. Sci.* **2007**, 6, 135

[37] Shirakawa, A.; Sakane, I.; Kobayashi, T. *Opt. Lett.* **1998**, 23, 1292

[38] Shirakawa, A.; Sakane, I.; Takasaka, M.; Kobayashi, T. *Appl. Phys. Lett.* **1999**, 74, 2268

[39] Baltuska, A.; Kobayashi, T. *Appl. Phys. B: Lasers Opt.* **2002**, 75, 427

[40] Bardeen, C. J.; Wang, Q.; Shank, C. V. *Phys. Rev. Lett.* **1995**, 75, 3410

[41] Kobayashi, T.; Baltuska, A. *Meas. Sci. Technol.* **2002**, 13, 1671

[42] Poprawa-Smoluch, M.; Baggerman, J.; Zhang, H.; Maas, H. P. A.; Cola, L. D.; Brouwer, A. M. *J. Phys. Chem. A* **2006**, 110, 11926

[43] Schmidt, B.; Sobotta, C.; Malkmus, S., Laimgruber, S.; Braun, M.; Zinth, W.; Gilch, P. *J. Phys. Chem. A* **2004**, 108, 4399

[44] Cerullo,G.; Lanzani, G.; Zavelani-Rossi, M.; De Silvestri, S. *Phys. Rev. B*, **2001**, 63, 241104

[45] Hagiri, M.; Ichinose, N.; Zhao, C.; Horiuchi, H.; Hiratsuka, H.; Nakayama, T. *Chem. Phys. Lett.* **2004**, 391, 297